Bifurcation Points for Tropical Cyclone Genesis and Intensification in Sheared and Dry Environments

CHAEHYEON C. NAM,[a] MICHAEL M. BELL,[a] AND DANDAN TAO[a,b]

[a] *Colorado State University, Fort Collins, Colorado*
[b] *University of Bergen, Bergen, Norway*

(Manuscript received 25 April 2022, in final form 9 June 2023, accepted 25 June 2023)

ABSTRACT: The combination of moderate vertical wind shear (VWS) and dry environments can produce the most uncertain scenarios for tropical cyclone (TC) genesis and intensification. We investigated the sources of increased uncertainty of TC development under moderate VWS and dry environments using a set of Weather Research and Forecasting (WRF) ensemble simulations. Statistical analysis of ensemble members for precursor events and time-lagged correlations indicates that successful TC development is dependent on a specific set of precursor events. A deficiency in any of these precursor events leads to a failure of TC intensification. The uncertainty of TC intensification can be largely attributed to the probabilistic characteristics of precursor events lining up together before TC intensification. The critical bifurcation point between successful and failed trials in these idealized simulations is the sustained vortex alignment process. Even for the failed intensification cases, most simulations showed deep organized convection, which reformed a midlevel vortex. However, for the failed cycles, the new midlevel vortex could not sustain vertical alignment with the low-level center and was carried away by VWS shortly. Under the most uncertain setup (VWS = 7.5 m s^{-1} and 50% moisture), the latest-developing ensemble member had seven events of tilt decreasing and increasing again that occurred during the 8 days before genesis. Some unsuccessful precursor events looked very close to the successful ones, implying limits on the intrinsic predictability for TC genesis and intensification in moderately sheared and dry environments.

SIGNIFICANCE STATEMENT: The aim of this study is to identify a critical bifurcation point that determines whether tropical disturbances in moderately sheared and dry environments will develop into intense storms or dissipate. When it comes to predicting the formation and strength of tropical cyclones, vertical wind shear, where the environmental wind changes with height, presents a challenging scenario. When the shear is neither too weak nor too strong, some systems manage to develop into cyclones, while others get torn apart under similar shear conditions. Understanding the differences between these outcomes remains a puzzle. Through extensive computer simulations, we have discovered a key factor that contributes to the uncertainty surrounding the alignment of the midlevel vortex with the center of the low-level vortex. These results reveal the complexity and multiple sources of uncertainty involved in forecasting tropical cyclone intensification, providing valuable insights into why moderate shear is a particularly challenging regime to predict tropical genesis and intensification.

KEYWORDS: Hurricanes/typhoons; Time series; Idealized models; Mesoscale models; Shear structure/flows

1. Introduction

Vertical wind shear (VWS) is one of the most important factors for tropical cyclone (TC) genesis and intensity change. Weak VWS provides a favorable environment for TC development, while strong VWS could disintegrate the TC vortex (e.g., Bracken and Bosart 2000; Nolan and McGauley 2012). Moderate VWS is defined as the range of VWS magnitudes that are neither too weak to have negligible impacts on TC intensity change nor too strong to completely thwart TC intensification with the range of 4.5–11 m s^{-1} (Rios-Berrios and Torn 2017). Both ensemble modeling studies and analyses of operational intensity forecast errors have shown that tropical cyclogenesis and intensification are the most unpredictable with moderate VWS (Zhang and Tao 2013; Finocchio and Majumdar 2017; Bhatia and Nolan 2013). The climatological study of Rios-Berrios and Torn (2017) also verified that the likelihood of intensifying or weakening is comparable with moderate VWS, whereas the likelihood is skewed toward intensification or weakening for weak and strong VWS, respectively.

Another factor that increases uncertainty around tropical cyclogenesis is environmental dry air. Moisture is essential to sustain diabatic convection and the associated vorticity generation and secondary circulation that intensify tropical cyclones, such that a drier atmosphere can suppress TC development. Studies comparing developing and nondeveloping tropical disturbances have found that a key difference between the two groups is the moisture, especially the midlevel humidity (Peng et al. 2012; Montgomery et al. 2012; Davis and Ahijevych 2013). The dry midlevel air affects the overall upward vertical mass flux via entrainment of less buoyant air parcels (i.e., radial ventilation; James and Markowski 2010) and convective downdrafts into the

Supplemental information related to this paper is available at the Journals Online website: https://doi.org/10.1175/JAS-D-22-0100.s1.

Corresponding author: Chaehyeon Chelsea Nam, c.chelsea.nam@colostate.edu

DOI: 10.1175/JAS-D-22-0100.1

subcloud layer (i.e., downward ventilation), which result in a longer recovery time for subsequent deep convection (Riemer et al. 2010; Alland et al. 2017). The combination of dry air and moderate VWS can further increase the uncertainties leading to TC genesis and intensification as alluded by Tang and Emanuel (2012) and Tao and Zhang (2014), with dynamic processes interacting with the thermodynamic processes of moistening (Tang et al. 2020). For example, the ventilation process is more efficient when the vortex tower is tilted by VWS as both radial and downward ventilation can more easily impact the inner-core convection (Alland et al. 2021a,b).

In this study, we aim to gain a process-based understanding of why the combination of moderate VWS and environmental dry air makes an uncertain setup for the early phase of TC development. A developing TC is at the border of two scales, the quasi-balanced synoptic scale and the stochastic cloud-organizing mesoscale (Ooyama 1982). Our hypothesis is that the stochastic character of diabatic convection becomes more important for TC genesis and intensification in marginally favorable environments such as moderately sheared and dry environments.

Recent observational and modeling studies have revealed that TCs that successfully develop or intensify under moderate to large VWS undergo vortex restructuring processes such as "downshear reformation" (Nguyen and Molinari 2015; Rios-Berrios et al. 2018; Chen et al. 2018; Nam and Bell 2021). The downshear reformation process starts with convection shifted to the downshear area by the VWS. Inside the convective area in the downshear region, the vertical component of vorticity is produced through tilting of horizontal vorticity, vortex stretching, and vertical advection of vorticity. The newly produced vorticity is accumulated inside the broader circulation through a vortex merger process. Thus, multiple thermodynamic and dynamic processes need to come together, namely, deep convection in the downshear region, vorticity generation, and vortex alignment through vortex merger. Then, our question is which processes may lead to bifurcation points between the TCs that do develop and the ones that do not intensify under the same magnitude of VWS.

Nine sets of idealized TC simulations with 20-member ensembles with varying VWS magnitude and environmental humidity are used to answer the above scientific question. Ensemble numerical simulations have been widely used by previous studies as means to investigate the intrinsic predictability of weather and TCs (e.g., Lorenz 1969; Melhauser and Zhang 2012). We investigated the TC characteristics leading to TC intensification: vertical realignment of the vortex tower, organized deep convection near the vortex center, and vortex strength (e.g., Wang 2012; Tao and Zhang 2014, 2015; Alland et al. 2021a). The rest of this paper is outlined as follows. Section 2 outlines the experimental design and the ensemble model setup. Section 3 describes the results from those simulations. Section 4 synthesizes the results and explores the underlying cause of the uncertainties for the marginally favorable environments, and discusses the implications of our findings from the idealized simulations for real TCs.

2. Experiment setup

Tropical cyclone interactions with VWS and a dry environment were simulated in this study with the Advanced Research version of Weather Research and Forecasting (ARW-WRF; Skamarock et al. 2008) Model (version 3.1.1). We note that the simulations analyzed in this paper were previously shown and analyzed from an ensemble mean perspective in Tao and Zhang (2014). We ran sensitivity tests with a newer version of WRF (3.9) and found that the initial vortices spin up earlier in WRF 3.9 compared to WRF 3.1.1 but the main mechanisms that we identify did not change [not shown; see Nam (2021) for details].

Three two-way nested domains were used with 18-, 6-, and 2-km horizontal grid spacing. The three domains contained 240 × 240, 240 × 240, and 360 × 360 grid points, respectively, which yields the domain sizes of 4320 km × 4320 km, 1440 km × 1440 km, and 720 km × 720 km. All domains had 40 vertical levels, with the model top at 20 km. The two inner domains were designed to follow the center of the vortex center at the 850-hPa level. The configuration and choice of physics packages included Yonsei University (YSU) boundary layer scheme (Hong et al. 2006) and WRF single-moment 6-class microphysics scheme (WSM6) (Hong et al. 2004). No cumulus parameterization nor short- or longwave radiation schemes were used in our simulations. Not including radiation could delay TC development (Rios-Berrios 2020) and exclude the impacts from diurnal pulses of convection (Dunion et al. 2014). We discuss sensitivities to radiation more in section 4.

For all simulations, a weak, warm-core vortex was prescribed in the initial conditions with a modified Rankine vortex profile having a set maximum tangential wind of 15 m s^{-1} at 850 hPa and 135-km radius. Tangential winds vanish at an 800-km radius and decay vertically following an exponential function (Moon and Nolan 2010). All simulations were set on a constant sea surface temperature (SST) of 29°C and a constant planetary vorticity (i.e., a doubly periodic f plane) corresponding to 20°N.

Around the tropical cyclone–like vortex, different profiles of environmental winds and thermodynamic soundings were specified. Figure 1 describes the environmental setup. Figure 1a shows the vertical profile of zonal winds that is prescribed for the simulations. For SH5, SH7.5, and SH10 configurations, westerly vertical wind shear (200–850 hPa) of 5, 7.5, and 10 m s^{-1} was imposed with a method of "point downscaling" developed by Nolan (2011). We note that the point-downscaling method forces VWS without imposing the temperature gradient induced by the shear and according to the thermal wind balance equation. With 10 m s^{-1} VWS and 720-km domain size, the maximum temperature difference is around 1°C, which is not negligible but still quite small [see appendix A of Tao (2015) for details].

For Moist100 simulations, the Dunion and Marron (2008) non–Saharan air layer (SAL) mean hurricane season sounding was used for the initial thermodynamic profile following Zhang and Tao (2013). The Dunion and Marron (2008) non-SAL mean sounding (calculated from 2002) is moister in the lower levels compared to the moist tropical sounding in Dunion (2011) (calculated from 1995 to 2002). To investigate the impact of environmental dry air, the initial field of water vapor mixing ratio was modified as shown in Fig. 1b, as the water vapor mixing ratio for all heights in outer-core regions (outside the radius of 300 km) is reduced to 50% and 25% of the Dunion non-SAL sounding for Moist50 and Moist25 sets. For all simulations, the moisture is the same in the inner-core regions (within a 200-km

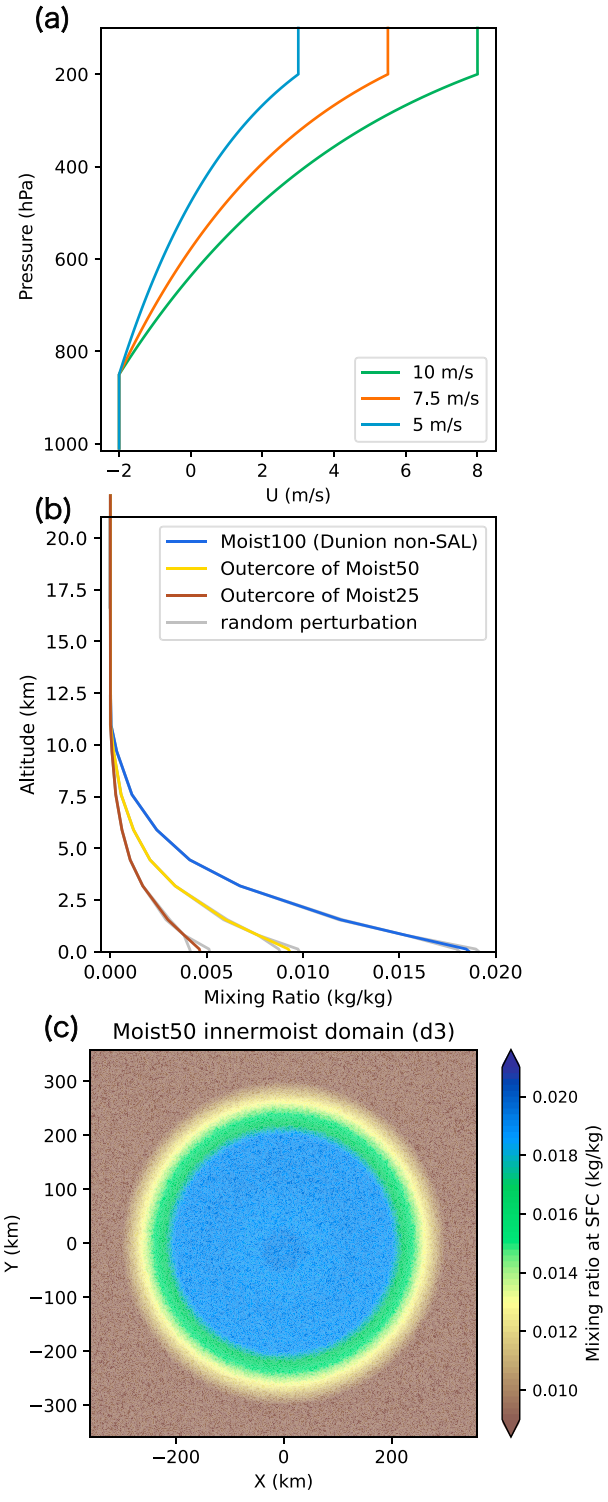

FIG. 1. Vertical profiles of (a) environmental zonal wind for SH5, SH7.5, and SH10 experiments and (b) water vapor mixing ratio for the outer-core region (≥300-km radius) for Moist100, Moist50, and Moist 25; (c) water vapor mixing ratio at the surface level from one of the Moist50 experiments.

TABLE 1. List of experiments with corresponding experimental setups.

Set name	Wind shear (m s^{-1})	Outer-core moisture
SH10_Moist100	10	Dunion non-SAL
SH10_Moist50	10	50% of Moist100
SH10_Moist25	10	25% of Moist100
SH7.5_Moist100	7.5	Dunion non-SAL
SH7.5_Moist50	7.5	50% of Moist100
SH7.5_Moist25	7.5	25% of Moist100
SH5_Moist100	5	Dunion non-SAL
SH5_Moist50	5	50% of Moist100
SH5_Moist25	5	25% of Moist100

radius), and between 200- and 300-km radii, the moisture decreased linearly (see Fig. 1c). Throughout the simulation hours, both the wind and water vapor fields are allowed to evolve from their initial values.

Each set of experiments consists of 20 ensemble members. The size of 20 ensemble members may not be enough to capture the full range of the possible outcomes, but our goal is not ensemble prediction of real TCs that should aim for the true spread. In this study, we aim to understand the physical factors that lead to increased uncertainty in TC genesis and intensification in marginally favorable environments. For that purpose, we chose 20 members consistent with previous idealized TC modeling studies (e.g., Rios-Berrios 2020; Tao and Zhang 2015). To generate the ensembles, small amplitude random moisture perturbations are introduced; the initial field of water vapor mixing ratio below 950 hPa was perturbed with random noise between −0.5 and 0.5 g kg^{-1} sampled from a uniform distribution (Zhang and Tao 2013; Judt et al. 2016). We have conducted sensitivity tests with more realistic dry soundings of SAL (Dunion 2011) and midlevel dry intrusion (Martinez et al. 2020) and the SAL runs were similar to the Moist50 set (not shown). More discussion about the sensitivity tests can be found in section 4.

With the three different shear profiles and three moisture profiles, there are, in total, nine different experimental sets to investigate the combined impacts of shear and dry air. Table 1 shows descriptions of all the ensemble sets analyzed in this study.

3. Results

a. *Overview of TC development*

In our study, the timing of TC genesis is determined as the timing of the simulation obtaining minimum sea level pressure (MSLP) below a threshold of 996 hPa as the onset of sustained intensification. It can be challenging to determine the exact timing of TC genesis for a simulated tropical disturbance. Tang et al. (2020) described TC genesis, based on WMO (2017), as "the development from a tropical disturbance—a discrete tropical (or subtropical) weather system of apparently organized convection—to a tropical depression (TD) or tropical storm (TS)—a warm-core, non-frontal, synoptic-scale cyclone with organized deep convection and a closed surface wind circulation about a well-defined center." This somewhat subjective definition highlights the lack of quantitative guidelines to identify TC

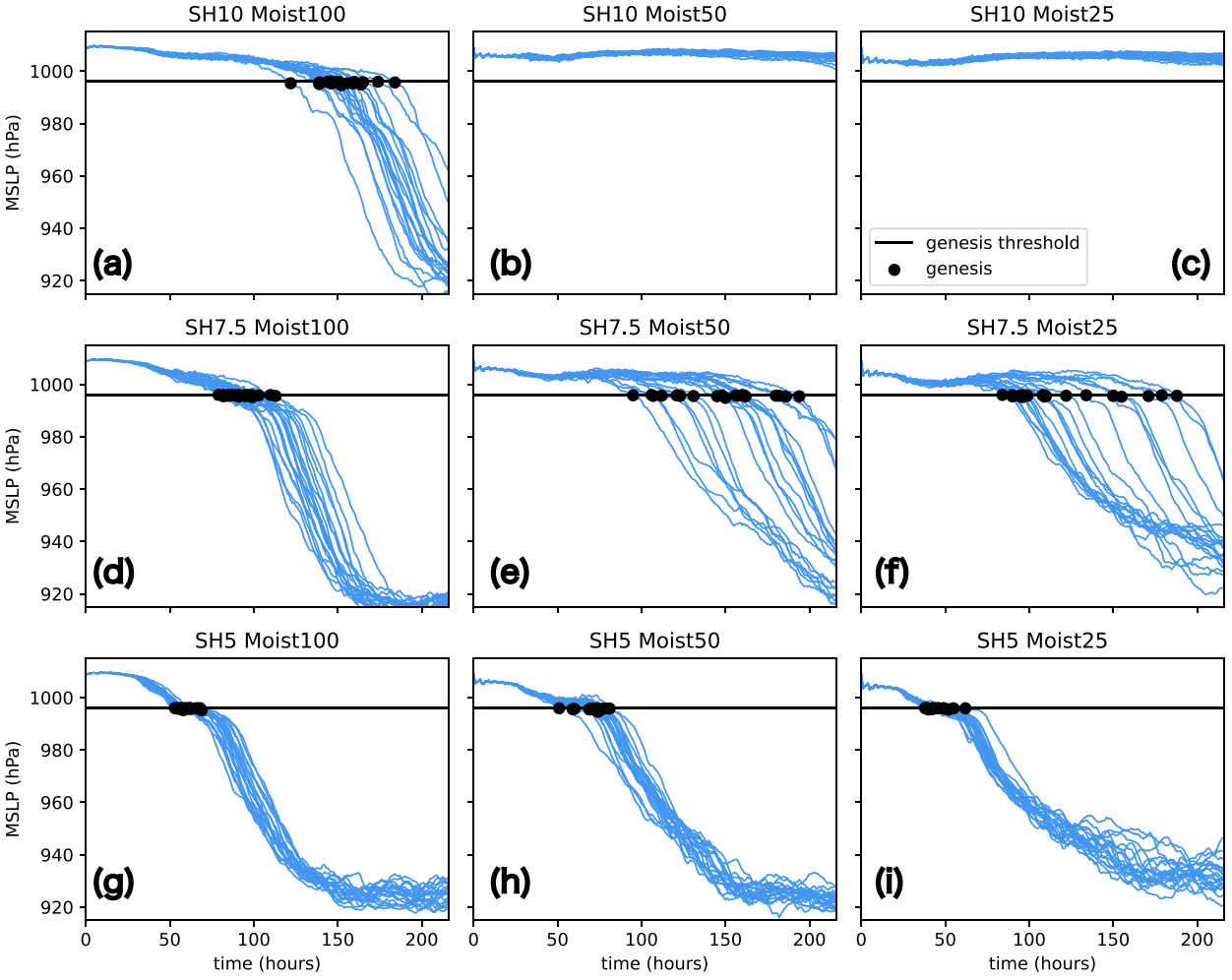

FIG. 2. Time series of hourly minimum sea level pressure for 20 ensemble members of nine experimental sets. Timings of tropical cyclogenesis are marked with black circles. Each time series is smoothed using a 12-h low-pass Lanczos filter with nine weights.

genesis. In the continuum of states of tropical intensity, we decided to use TS designation (when the TC is named if it were a real storm) to define the genesis time for each simulated TC similar to previous TC genesis studies (Bell and Montgomery 2019; Murthy and Boos 2018). The guidance of Dvorak CI number of 2.5, which corresponds to the transition from TD to weak TS, correlates with 13-hPa deficit of central pressure (ΔP) (Knaff and Zehr 2007; Courtney and Knaff 2009). In our idealized simulations, the environmental SLP (the initial SLP of the outermost domain far enough from the initial vortex) was uniform around 1009 hPa, so 996 hPa corresponds to 13 hPa of ΔP compared to the environments. We decided to use MSLP rather than maximum wind speed to measure TC genesis and intensification because the central pressure deficit is an intensity measure that combines maximum wind speed, storm size, and background rotation rate (Chavas et al. 2017), and is easier to estimate and more stable with time than maximum wind speed (Klotzbach et al. 2020).

VWS and dry air together have profound impacts on the evolution of simulated tropical cyclones. Figure 2 displays the time series of MSLP for the nine ensemble sets. For all ensembles, the simulated tropical cyclones undergo only minimal MSLP deepening during the first 36 h. Substantial differences depending on VWS and environmental humidity appear after the first 36 h. In general, the weaker VWS and the more moisture, the earlier ensembles develop. The average timing of genesis for the three SH5 sets is similar (see Figs. 2g–i). Most of the SH5 ensembles reach a steady state of MSLP around 150 h and the steady-state MSLP is lower in the moister simulations through the simulation time (Figs. 2g–i). For the strongest VWS of 10 m s^{-1}, only the ensembles with Moist100 underwent genesis during the 9 days of simulation time, and no ensembles from SH10_Moist50 and SH10_Moist25 reached a point of tropical cyclogenesis (Figs. 2a–c). SH7.5_Moist100 is right in between SH5_Moist100 and SH10_Moist100 in terms of genesis timing and ensemble spread (Fig. 2d).

The largest ensemble spread was found in the drier sets of SH7.5 (Figs. 2e,f). The standard deviation of MSLP from 20 ensemble members of SH7.5_Moist50 was 18.8 hPa at median genesis time (153 h) and reached a maximum of 23.2 hPa at

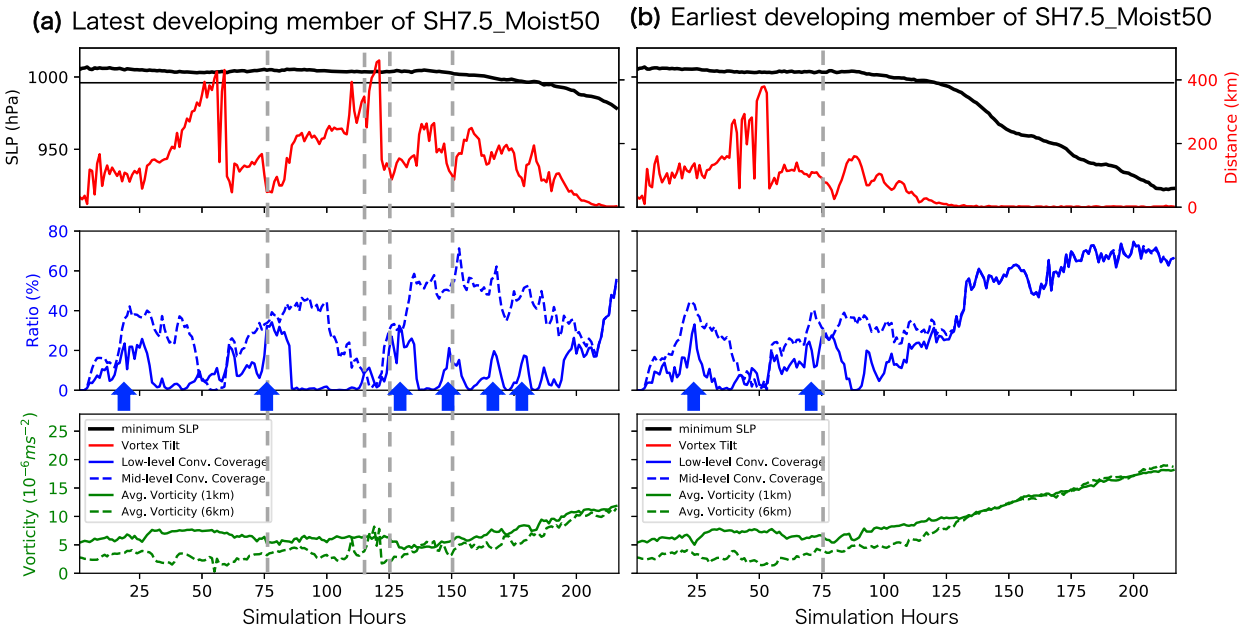

FIG. 3. Time series of variables show thermodynamic and dynamic processes leading to intensification for (a) latest-developing ensemble member and (b) earliest-developing ensemble member of SH7.5_Moist50 experimental set. Blue arrows mark distinctive low-level convective bursts. Gray dashed lines indicate the time steps (hour 75, hour 115, hour 125, hour 150) highlighted in Figs. 5–8 for latest member and the time step of hour 75 in Fig. 4 for the earliest member.

191 h. The second largest ensemble spread was found from SH7.5_Moist25 with a maximum of 21.7 hPa at 166 h. For SH10, the dry environment simply eliminated the possibility of TC development, and for SH5, the ensemble spread was still pretty narrow (maximum 6.3 and 6.2 hPa for SH5_Moist50 and SH5_Moist25), not so different from Moist100 simulations (maximum 7.0 hPa). In contrast, for SH7.5, having a drier environment made the ensemble spread of the MSLP time series much larger, which implies a difficult forecast problem; minimal amounts of random water vapor perturbation produced completely different TC development scenarios with 99-h difference in genesis timing between the earliest-developing member and the latest-developing member of SH7.5_Moist50.

b. *Bifurcation points for TC intensification for SH7.5_Moist50*

We looked into each ensemble member under the experiment that showed the widest ensemble spread, the moderately sheared and dry environment of SH7.5_Moist50, to investigate how the minimal random perturbations could produce such a wide gap in the timing of TC genesis. In Fig. 3, we contrast the latest and the earliest-developing members of SH7.5_Moist50 set similar to Rios-Berrios et al. (2016), who analyzed TC intensification of Ophelia (2011) comparing strong and weak ensemble members. In addition to MSLP, the time series of vortex tilt, inner-core convective coverage (low level and midlevel), and average vorticity (low level and midlevel) are shown. Here, low level refers to 1-km altitude, and midlevel refers to 6-km altitude.

It is necessary to explain how we calculated these variables to lay out what each variable represents. All variables were interpolated in the vertical coordinate from the WRF sigma levels to altitude (from 0 to 22 km in a 400-m interval) using the geopotential height and pressure outputs. First, the vortex center at each vertical level is detected as the location of minimum pressure with the pressure field smoothed with a Gaussian filter with sigma (the standard deviation for Gaussian kernel) of 10 grid points. We confirmed that our findings hold when the vortex centers are calculated using the pressure centroid method (Nguyen et al. 2014). Second, convective coverage indicates the proportion of area inside the inner-core region (200 km × 200 km box around the vortex center) that is covered by convection. We used 20 dBZ at a 6-km altitude as the threshold to indicate a convective grid cell (Rogers et al. 2015). The low-level convective coverage indicates the convective coverage of the 200 km × 200 km box around the vortex center at 1 km, and the midlevel convective coverage is measured inside the 200 km × 200 km box around the vortex center at 6 km [e.g., panels (b) and (d) of Figs. 5–8]. Thus, the low-level and midlevel convective coverage will be identical if the vortex tilt is zero as the two boxes overlap. Last, the average vorticity is the arithmetic mean of the relative vertical vorticity inside the 200 km × 200 km domain surrounding the vortex center at the respective altitudes of 1 and 6 km. When the vortex tilt is large (>260 km), the 200 km × 200 km midlevel box can be cut off at the edge of the inner domain, and for this case, the midlevel metrics are calculated over the smaller rectangular box (see Figs. 6a,c).

Comparing the two panels of Fig. 3 through the first 90 h, the two ensemble members exhibit a similar evolution. The

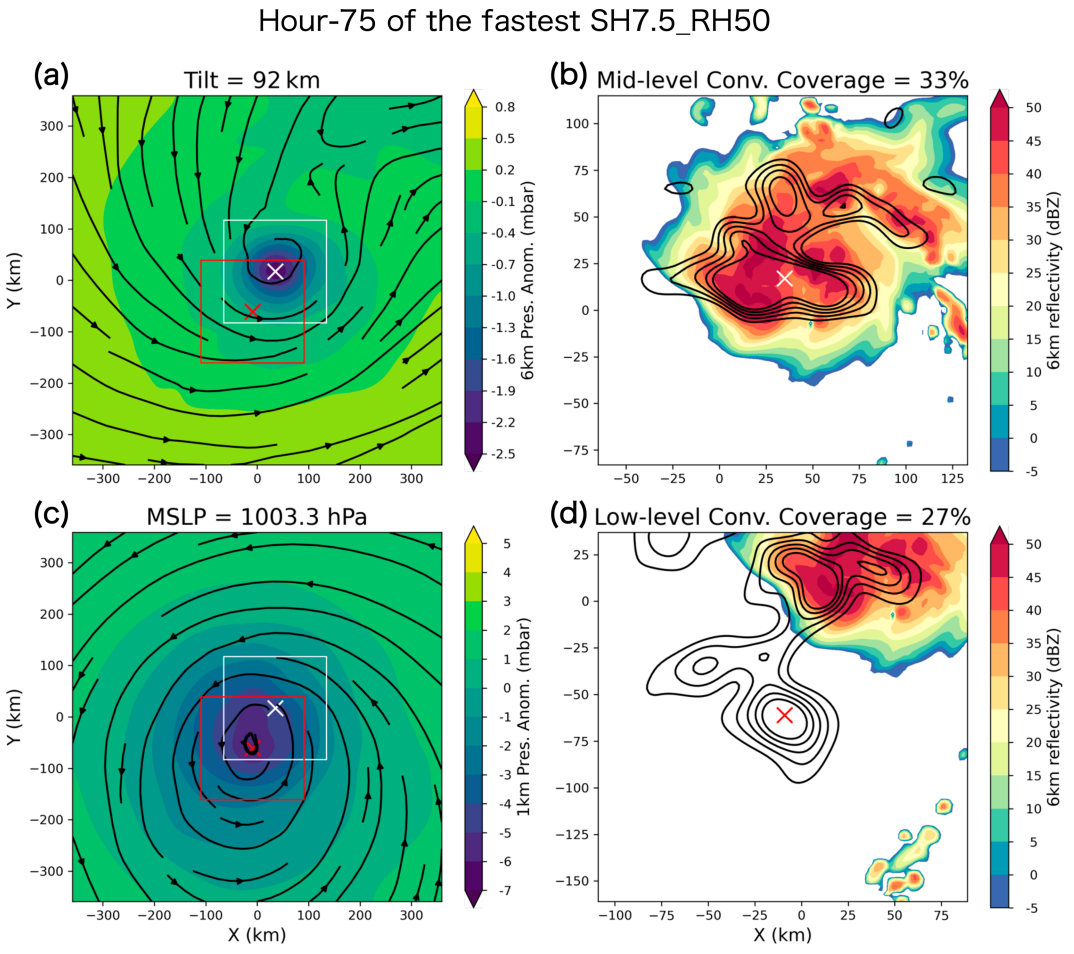

FIG. 4. Snapshot of simulated TC from the earliest-developing member of SH7.5_Moist50 at hour 75 (dashed line in Fig. 3b). Pressure anomaly and the streamlines at an altitude of (a) 6 km and (c) 1 km; simulated reflectivity at 6 km inside the 200 km × 200 km box around the center of (b) midlevel vortex center (defined at 6 km) and (d) low-level vortex center (defined at 1 km). Relative vorticity at 6 and 1 km is plotted in black contours in (b) and (d) from 1×10^{-5} to 3×10^{-5} s^{-1} in the interval of 5×10^{-6} s^{-1}. Red and white × markers indicate the low-level and midlevel vortex centers, respectively. The 200 km × 200 km red and white boxes in (a) and (c) are centered on the low- and midlevel vortex centers. The white box is zoomed in as the domain of (b), and the red box corresponds to the domain of (d).

vortex tilt increased and rapidly decreased with changing convective coverage. For the latest-developing member, multiple cycles [six cycles when counting each distinctive low-level convective burst (see blue arrows in Fig. 3)] occurred before genesis, whereas the earliest-developing member reached tropical cyclogenesis after going through two cycles. Here, one cycle of the precursor event is defined as the precursor variable reaching a certain threshold and maintaining the magnitude for more than three hours before the precursor event terminates. How we set the specific thresholds for different precursor variables will be described in section 3c.

The first convective cycle spanned about 48 h for both members. Initially, convective coverage increased in the inner-core region in the first 36 h. As the vortex tilt increased while the midlevel vortex was shifted eastward by westerly VWS, there emerged a discrepancy between low-level and midlevel convective coverage. Low-level convective coverage decreased from 20% to 0% as tilt increased, but midlevel convective coverage remained relatively constant at 35% for a longer time.

For both ensemble members, the second cycle started around 55 h, with convective coverage starting to increase again, and then around 60 h, vortex tilt drastically decreased from 400 km to below 50 km. With the midlevel vortex being displaced 400 km from the low-level vortex center, it is probably more accurate to consider these two distinct vortices rather than a vertically coherent tilted vortex. Similar to the first cycle, as tilt increased again, low-level convective coverage decreased around 85 h. The bifurcation point between these two members appears to be around 90 h: the latest member's tilt kept increasing but the earliest member's tilt started to diminish again. As tilt approached zero (midlevel and low-level vortices perfectly aligned), the earliest-developing member quickly passed the genesis phase and entered the rapid intensification phase. The latest-developing member took more cycles of tilt

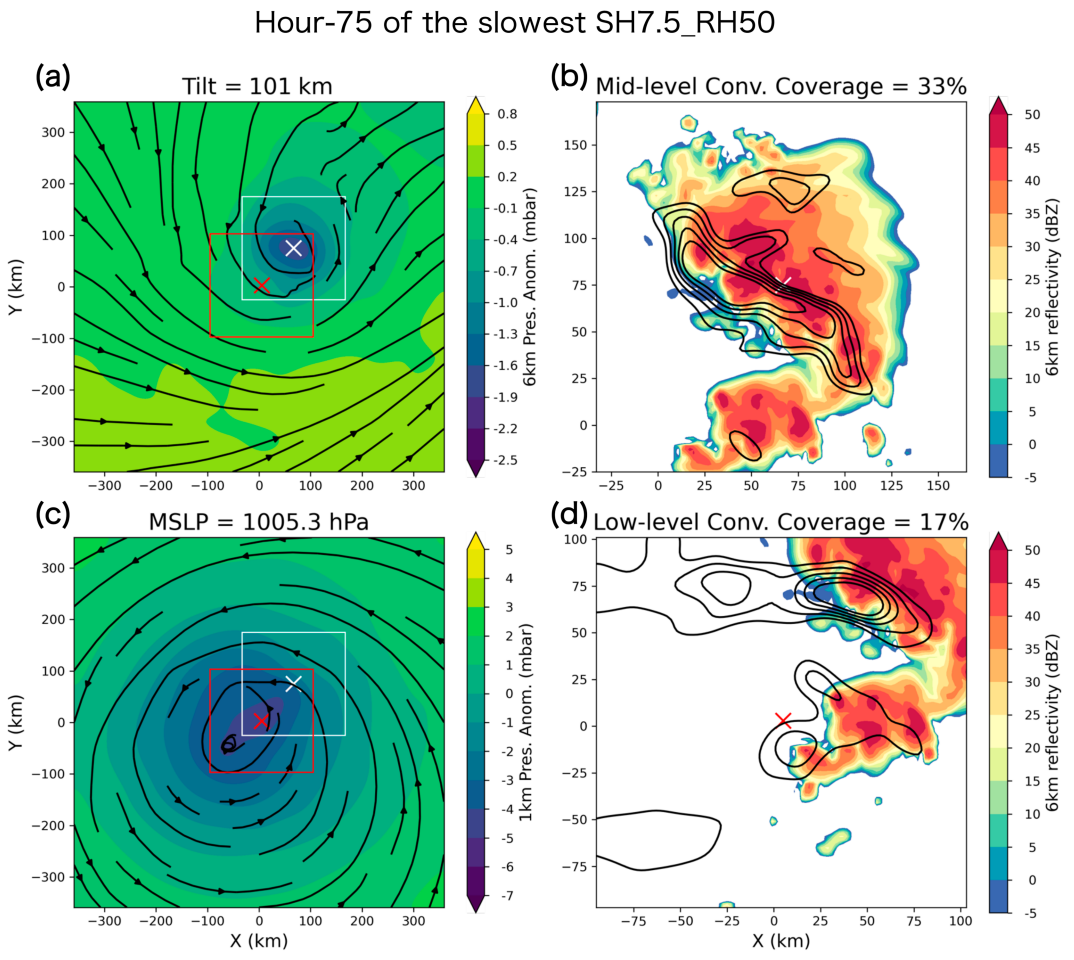

FIG. 5. As in Fig. 4, but from the latest-developing member at hour 75 (dashed line in Fig. 3a).

decreasing and multiple low-level convective coverage bursts until it underwent genesis.

The average low- and midlevel vorticity steadily increase in concert with the steadily decreasing trend of MSLP for both the earliest and latest-developing members. In Fig. 3b, the midlevel vorticity starts from a lower magnitude compared to the low-level vorticity but increases faster than the low-level vorticity; they reach a similar magnitude of vorticity in about 24 h after the low-level vorticity starts to increase.

We examined the hourly pressure and reflectivity fields of the two ensemble members to investigate the detailed process behind the repeated cycles of precursor events. Figures 5–8 show the snapshots of the simulated TC of the latest ensemble member of SH7.5_Moist50 at hour 75, hour 115, hour 125, and hour 150, respectively (gray dashed lines in Fig. 3a). To compare with Fig. 5, Fig. 4 shows the snapshot of the earliest ensemble member at the same simulation hour 75 and its second cycle of convective bursts. The hour-75 and hour-150 time steps are peaks in the low-level convective coverage of the second and fourth cycles for the latest-developing member. The hour 115 and hour 125 mark the times before and after the drastic tilt decrease during the early phase of the third cycle of the low-level convective bursts.

Figure 4 displays the pressure deficit and reflectivity at both the low level (1 km) and midlevel (6 km) for the earliest ensemble member at hour 75. As expected with the westerly VWS, a midlevel vortex appears northeast of the low-level vortex center (white × and red ×, respectively, in Figs. 4a,c). The tilt was relatively small (92 km), and a mesoscale convective system was situated at the center of the midlevel vortex. The midlevel vorticity contours align with deep convection within the mesoscale convective system (Fig. 4b). In contrast, at the same hour 75, the latest ensemble member has a local maximum of low-level convective coverage. Despite this difference, Figs. 4 and 5 share similar characteristics in terms of the downshear left location of the midlevel vortex and the same 33% of midlevel convective coverage. However, the earliest member has a broader low-level convective coverage and stronger low-level vorticity. Notably, the tilt was 101 km for the latest-developing member. A mesoscale convective system was present at the center of the midlevel vortex. The midlevel vorticity contours correspond with deep convection within the mesoscale convective system (Fig. 5b). Taken together, Figs. 3–5 suggest that at hour 75, it is challenging to predict which TC will develop in 36 h and which will not develop for 4 days.

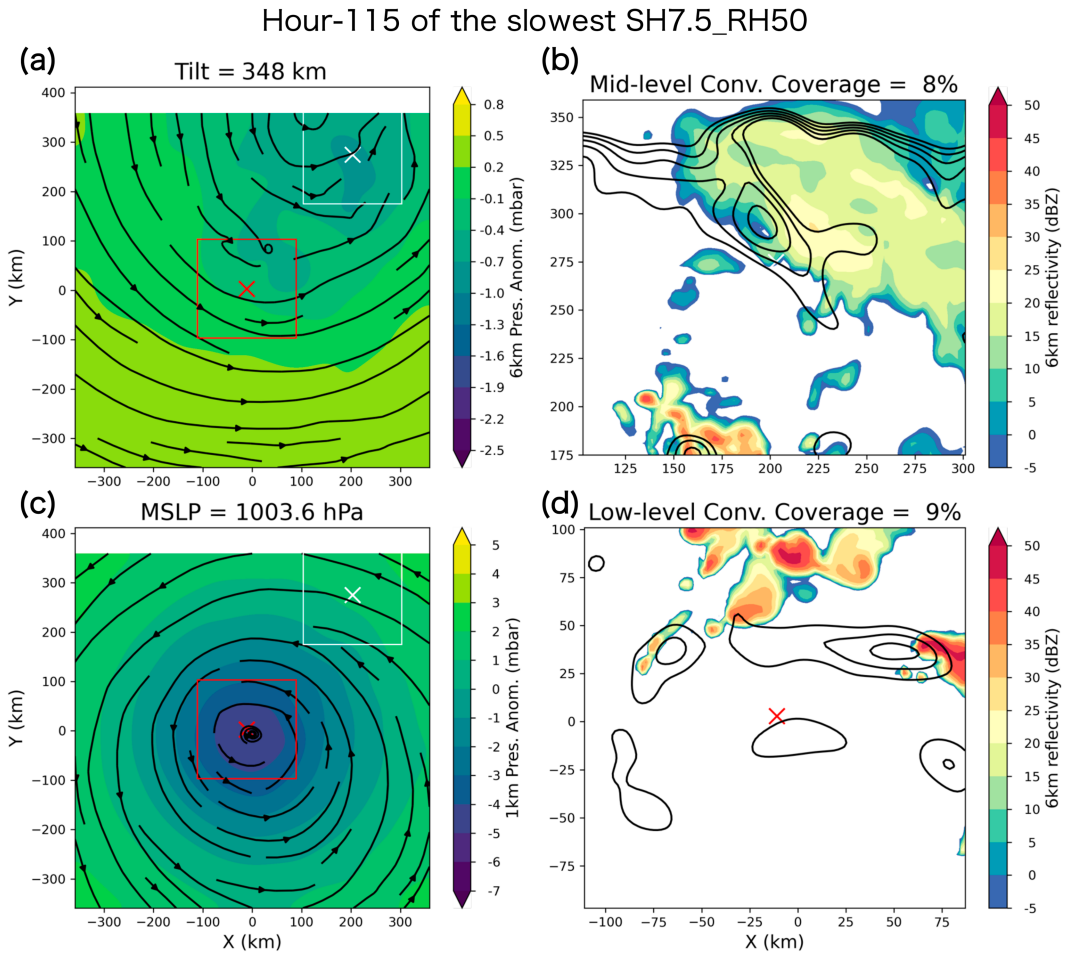

FIG. 6. As in Fig. 4, but from the latest-developing member at hour 115 (dashed line in Fig. 3a).

Figure 6 shows, for the latest-developing member, that the midlevel vorticity shown in Fig. 5 was carried away northeastward by the westerly VWS. The 200 km × 200 km boxes centered around the midlevel and low-level vortex centers have much smaller convective coverage and vorticity not well aligned with convection. Ten hours later (in Fig. 7), the vortex tilt had decreased drastically because a new smaller midlevel vortex formed inside the deep mesoscale convective system. Looking at the hourly output of reflectivity, pressure, and vorticity fields at the midlevel (not shown), we confirmed that after the preexisting midlevel vortex is advected away by the VWS, a new smaller-scale (meso-beta-scale) midlevel vortex forms at the same location of the deepest convection in downshear left quadrant, likely through vortex stretching by the deep convection. The idealized simulations of tilted TCs in Schecter and Menelaou (2020) also showed that tilt increase can be explained by adiabatic mechanisms, but tilt decrease can only be explained with the diabatic processes around the mesoscale convective systems.

From hour 125 to the time of TC genesis, the tilted vortex went through a prolonged vortex alignment process. The tilt kept fluctuating but never reached 400-km magnitude like before. From hour 125 (Fig. 7) to hour 150 (Fig. 8), the midlevel pressure deficit became larger, and the midlevel circulation became more robust, centered around the new midlevel vortex center. Midlevel convective coverage also grew larger.

A key question is why the newly formed midlevel vortex at the second cycle (Fig. 5) did not result in TC intensification and was carried away, whereas the midlevel vortex at the fourth cycle (Fig. 8) persisted and resulted in intensification after the prolonged alignment process. Comparing Figs. 5 and 8, vortex tilts at these two times have similar magnitudes of 101 and 103 km, and the midlevel vortex is located northeast and east to the low-level vortex for hour 75 and hour 150. At both times, deep organized convection is located around the midlevel vortex center. One noticeable difference is that the midlevel vortex in hour 150 has a larger cyclonic circulation (see streamlines of Figs. 5a and 8a). While the increased size of the circulation may play a role, we have not done a detailed analysis of this factor. Further investigation into the specific characteristics that promote sustained vortex alignment is an important topic for future research.

The findings to highlight from Figs. 3–8 are as follows:

- The earliest-developing member and the latest-developing member have similar behavior of precursor events until the 90-h mark.

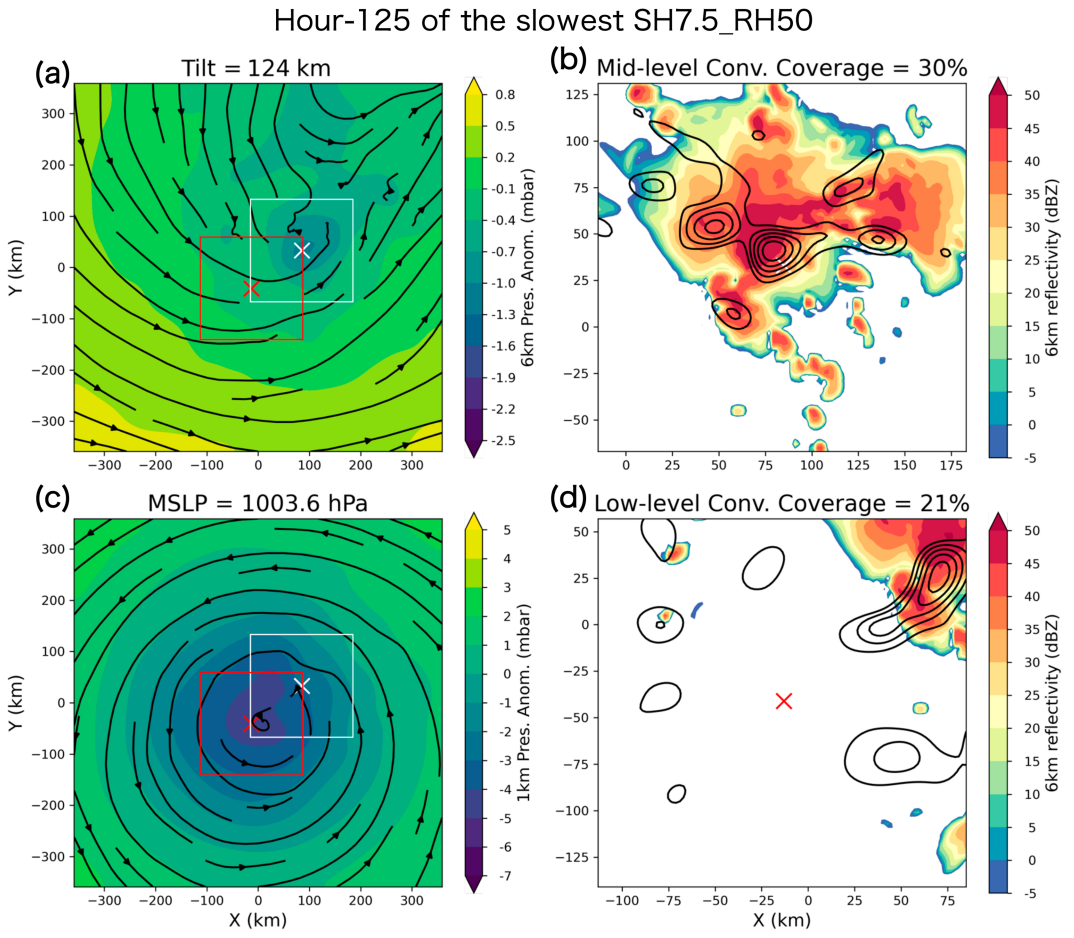

FIG. 7. As in Fig. 4, but from the latest-developing member at hour 125 (dashed line in Fig. 3a).

- The latest-developing member has multiple attempts at increasing convective coverage around the low and midlevel vortex centers that could possibly lead to TC intensification. Still, they all failed until the sixth attempt.
- Only after vortex tilt decreases closer to zero, SLP starts to drop rapidly.
- Low-level convective coverage is more episodic compared to midlevel convective coverage, and midlevel convective coverage persists for a longer time after tilt increases again.
- Midlevel vorticity shows hints of increasing slightly sooner than low-level vorticity increasing and SLP decreasing.
- Deep convection over a wider area inside the inner-core region generates a smaller-scale midlevel vortex, which results in an instantaneous vortex tilt decrease.
- A key difference between the successful and failed precursor cycles in SH7.5_Moist50 ensembles is whether the newly generated midlevel vortex sustains the alignment with the low-level vortex or it is advected away by the VWS again.

c. *Probabilistic approach to TC intensification*

We found the difference between the earliest and latest-developing members of the most uncertain ensemble set (SH7.5_Moist50) was how many cycles of increasing convective coverage and decreasing vortex tilt they go through to have a successful TC intensification. Now, our question is whether there exist physical differences between the successful and unsuccessful cycles of these precursor events. Due to the stochastic characteristic of convective initiation and complicated multiscale interactions between convection and the sheared environment (e.g., Nam and Bell 2021), the predictability of tropical cyclone intensification in this particular environment could be limited when using deterministic methods. In response to this inherent uncertainty, we adopted a probabilistic approach to quantify the number of precursor event trials necessary to achieve tropical cyclone intensification in each ensemble member.

Our probabilistic approach is inspired by the statistical model of the geometric distribution, which is the probability distribution of the number of Bernoulli trials needed to get one success. A famous example would be how many trials of coin flipping are required to get the tail side of the coin. In our case, each Bernoulli trial will be a precursor event, such as tilt decreasing below a certain threshold, and the success is TC genesis (i.e., MSLP reaching 996 hPa). Bernoulli trials are assumed to be independent, but we note that each precursor event cannot be purely independent of the other; the vorticity

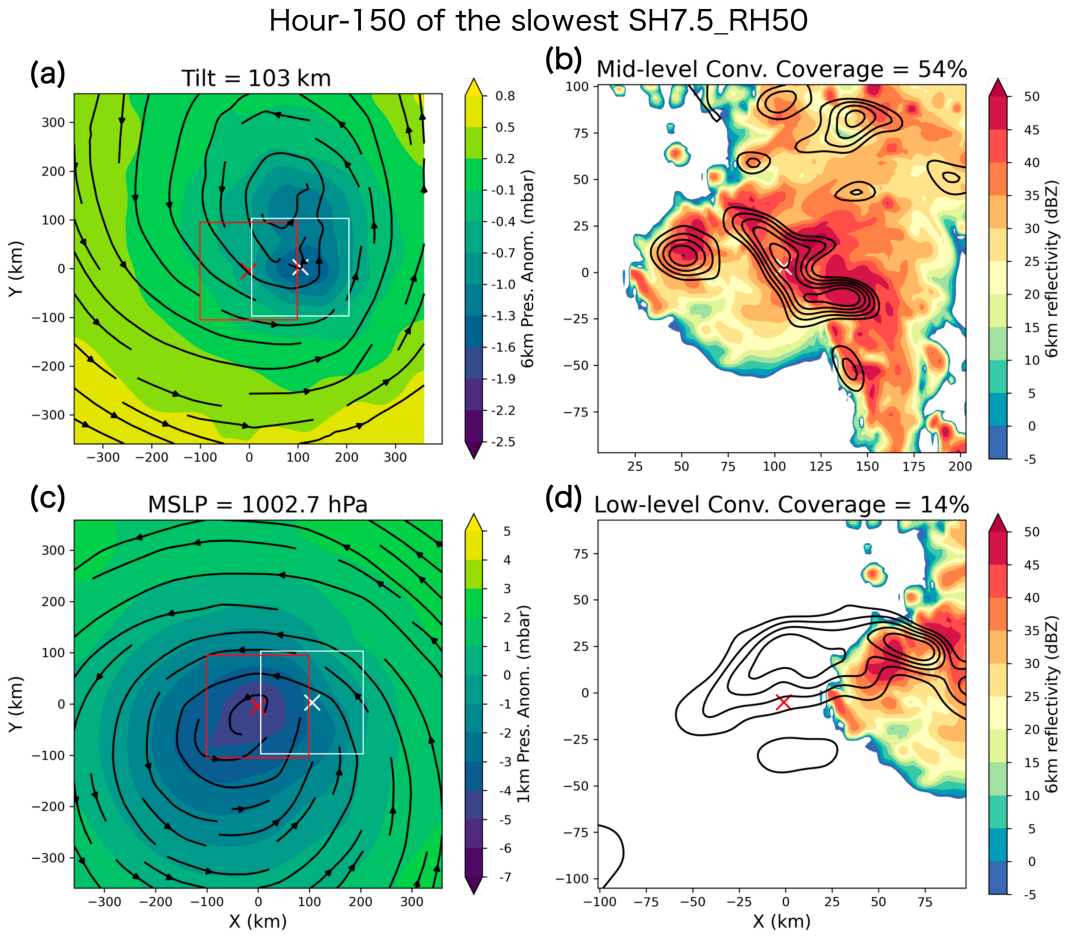

FIG. 8. As in Fig. 4, but from the latest-developing member at hour 150 (dashed line in Fig. 3a).

or moisture produced by previous convective bursts primes the environment for subsequent convective bursts. For example, the latest-developing member of SH7.5_Moist50 had a larger midlevel circulation and a lower SLP at the beginning of its fourth cycle compared to the second cycle (Figs. 5 and 8). Therefore, we quantitatively assessed the importance of the repeated trials of key physical processes leading to TC intensification, but because of the interdependence of precursor events we did not directly fit the data to a geometric or other probability distribution.

We used four precursor variables of vortex tilt magnitude, inner-core average midlevel vorticity, inner-core low-level convective coverage, and inner-core midlevel coverage to diagnose vortex misalignment, vortex intensity, and convective organization. We set the threshold of each precursor variable as the mean value of the variable at the genesis timing for all 140 developing members (except for 40 members of SH10_Moist50 and SH10_Moist25). The thresholds for the four precursors of vortex tilt magnitude, inner-core average midlevel vorticity, inner-core low-level convective coverage, and inner-core midlevel coverage are $<$82.0 km, $>6 \times 10^{-6}$ s^{-1}, $>$14.0%, and $>$37.0%, respectively (black lines in Fig. 9). We count it as a precursor event for each variable when that variable passes the threshold for at least 3 h. For example, if the vortex tilt was above 82 km at hour H and decreased below 82 km at hour $H + 1$, and the vortex tilt continued to be below 82 km until hour $H + 3$, we count it as a distinct tilt-decreasing precursor event.

The spread of data points of each precursor variable at genesis time indicates reaching a threshold does not guarantee TC intensification (colored dots in Fig. 9). Our choice of threshold is a tool to count the distinctive episodes of tilt decrease or convective bursts as shown in Fig. 3 for a fair comparison for all developing ensemble members. We confirmed that the method of using the median as a threshold instead of the mean did not affect the statistical results. We also tested the sensitivity of statistics using different thresholds for each ensemble set (colored horizontal lines in Fig. 9). The results were generally the same except for the SH10 ensemble sets because SH10_Moist100 is the outlier having a larger tilt and midlevel convective coverage and smaller low-level coverage (see green dots and lines in Fig. 9).

We analyzed saturation fraction as a candidate for precursor variable for TC intensification because previous studies have shown that sufficient saturation fraction above 80%–85% is essential for TC genesis and intensification (Nolan et al. 2007;

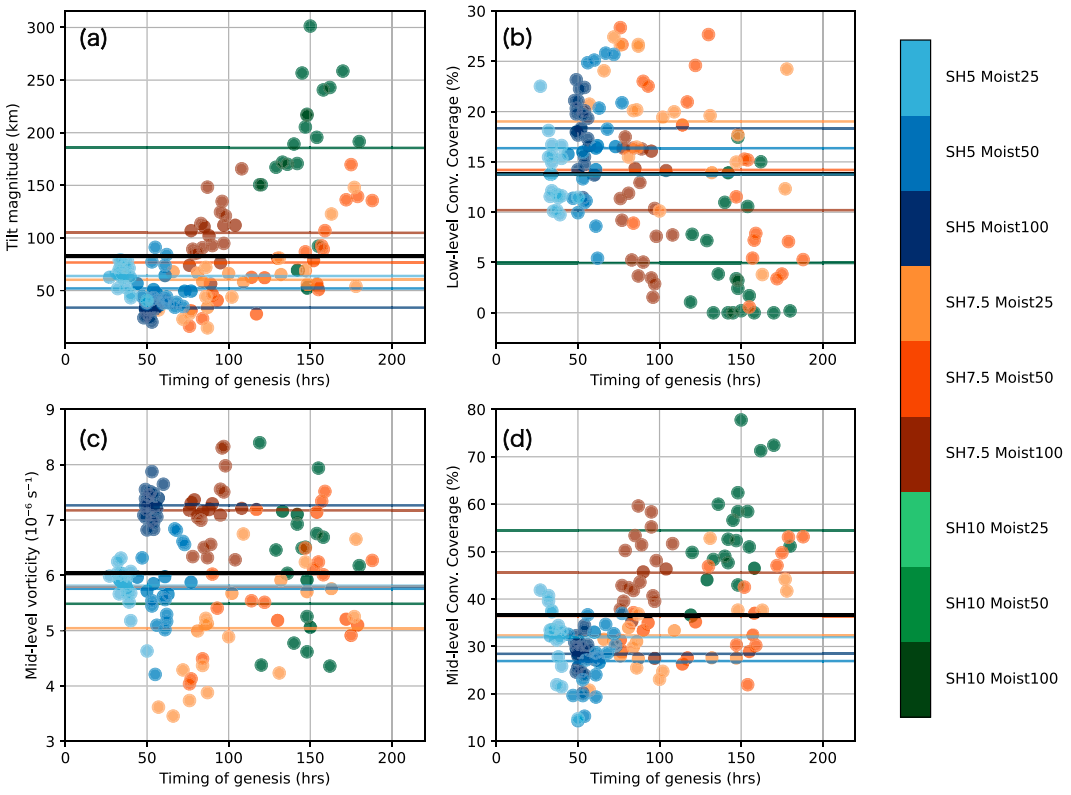

FIG. 9. The magnitude of the four TC intensification precursor variables of (a) vortex tilt magnitude, (b) low-level convective coverage, (c) average midlevel vorticity, and (d) midlevel convective coverage at genesis time for each ensemble member that underwent intensification during the 9-day simulation time. Horizontal lines indicate the average value for each color-coded ensemble set. The thicker black line is the average value of all 140 ensemble members at genesis timing, which was used as the threshold to count the number of precursor events: 82 km for vortex tilt, 14% for low-level convective coverage, 6×10^{-6} s^{-1} for inner-core midlevel vorticity, and 37% for midlevel convective coverage.

Raymond et al. 2014; Bell and Montgomery 2019). Figure 10 displays the saturation fraction at genesis time for all ensemble members of the nine sets. Saturation fraction is calculated as the integrated mass-weighted mixing ratio divided by the integrated mass-weighted saturation mixing ratio over the vertical layers between the surface and 6 km (Raymond and Kilroy 2019).

We found the saturation fraction threshold varies a lot depending on the size of the computation domain. The saturation fraction value at the timing of genesis varies from about 50% to 80% (for 720-km domain size) and from 75% to 89% (for 200-km domain size) depending on the shear and humidity configurations. For the 720-km box average, among the dry sets (Moist50 and Moist25), SH5 sets have the lowest saturation fraction, and SH10 sets have the highest domain average saturation fraction. It appears that simulated TCs of the SH5_Moist50 and SH5_Moist25 sets contain the moisture and heat energy in the inner-core region of the storm and utilize it efficiently to spin up the vortex, whereas the drier sets, under VWS 10 m s^{-1}, have moisture spread over a larger area shortly after it is produced by convective activities. Thus, the larger domain of the drier sets of SH10 becomes moister and moister but the vortex cannot intensify, and pressure cannot deepen. More importantly, a significant saturation fraction increase appears to occur after the TC genesis for most of the ensembles (online supplemental Figs. 4 and 5), which means saturation fraction increase follows TC genesis rather than leading to it. Thus, we did not use saturation fraction increase as a precursor event. However, inner-core moistening occurred in the first 36 h of initial spinup for all ensemble members regardless of shear and moisture setup, and moistening the inner-core can be a necessary condition that happens well before genesis. We did not examine the asymmetric ventilation or moistening around the convective area (Alland et al. 2021a; Alvey and Hazelton 2022), which may be more important for TC genesis than the domain-averaged humidity.

Figure 11 shows the number of precursor events before TC genesis. A key takeaway from Fig. 11 is that the marginally favorable environments of SH7.5_Moist50 and SH7.5_Moist25 have the most attempts of precursor events (up to seven times) among all the experiments. Note that the precursor events count based on the thresholds in Fig. 9 are different from how we subjectively annotated the cycles of convective bursts from Fig. 3. For the Moist100 sets in the left column of

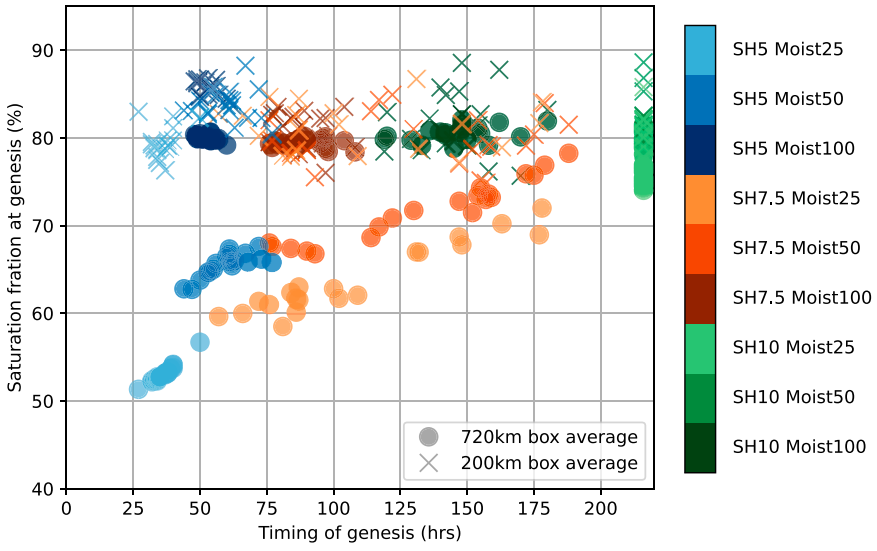

FIG. 10. Domain-averaged saturation fraction at genesis vs time of genesis. Circles denote the saturation fraction averaged in the 720 km × 720 km box centered around the low-level vortex, and crosses are for the 200 km × 200 km box centered around the low-level vortex. Data points of nondeveloping ensemble members of SH10_Moist25 and SH10_Moist50 are at hour 216.

Fig. 11, the three sets show similar distributions for midlevel vorticity increase and low-level convective coverage (Figs. 11c,e). For tilt decrease (Fig. 11a), all of the SH10_Moist100 and a majority of SH7.5_Moist100 ensemble members reached the point of TC genesis with midlevel and low-level vortex centers misaligned by farther than 82 km (Fig. 9a). Moist100 provides a very favorable thermodynamic setup of sea surface temperatures of 29°C and moist tropical sounding; thus, it is likely that simulated TCs under Moist100 can afford a larger magnitude of vortex tilt. Moist50 and Moist25, on the other hand, have a region of drier air in the outer-core region that can easily be brought into the inner-core region through radial ventilation if the vortex tower is tilted (Fig. 11b). Then, Fig. 11g shows that stronger VWS environments required more repetitions of midlevel convective coverage increasing beyond 37%, implying a lower success rate of the midlevel convective bursts leading to TC intensification in a stronger VWS condition.

Among SH7.5 sets, it is the drier experiments that have the widest spread of the number of precursor events that are required to reach TC genesis (Figs. 11b,f,h). The wide spread of the number of precursor events for the ensemble sets having a combination of moderate VWS and dry air is directly related to uncertainties in predicting genesis time or intensification onset. Midlevel vorticity increase, in general, has smaller numbers of attempts compared to the other variables because averaged vorticity increases more gradually than episodically (cf. Fig. 3).

Figure 12 displays the timing of the four precursor events against the timing of TC genesis for each ensemble member. There are many overlaps of the circles in each panel of Fig. 12 because all 140 developing members are shown, and many of the members underwent more than one precursor event before genesis. Vortex tilt decrease and low- and midlevel convective coverage increase exhibit a repeated cycle (see the orange arrows moving upward on y axis of Fig. 12). An initial convective burst occurs in the first 24 h of model spinup time (Figs. 12b,d). The second cluster of bursts occurs between 50 and 75 h. Then the following episodes occur between 100 and 175 h (if TC genesis did not happen until that point). The timing of midlevel vorticity increase almost coincides with the timing of genesis, only a few hours earlier. As discussed above, for vortex tilt, the reason why there are no data points of SH7.5_Moist100 and SH10_Moist100 is these ensembles reach TC genesis with vortex tilt larger than our threshold of 82 km (Fig. 9a). We conjecture that the TCs in these two ensemble sets intensify relying on the favorable thermodynamic environments despite the large magnitude of tilt (see large midlevel convective coverage in Fig. 9d and many midlevel convective burst events in Fig. 11g for SH10_Moist100).

The precursor event that has the longest lead time before TC genesis appears to be midlevel convective coverage increase, especially for SH7.5_Moist50 and SH7.5_Moist25, which are the ensemble sets that have the widest ensemble spread (see the distance between $y = x$ line and the orange circles in Fig. 12). For SH7.5_Moist50 and SH7.5_Moist25, the latest occurrence of midlevel convective coverage increasing beyond 37% before TC genesis happens, on average, 31.4 and 34.4 h prior to genesis time, respectively. On the other hand, the latest occurrence of low-level convective coverage increasing beyond 14% before genesis happens, on average, 15.6 and 8.7 h prior to genesis time for SH7.5_Moist50 and SH7.5_Moist25, respectively. It is consistent with Fig. 3 that showed midlevel convective coverage has more persistence than low-level convective coverage when tilt is amplifying again.

This section focused on analyzing the probabilistic characteristic of TC intensification under marginally favorable environmental conditions. Our findings revealed that each simulation

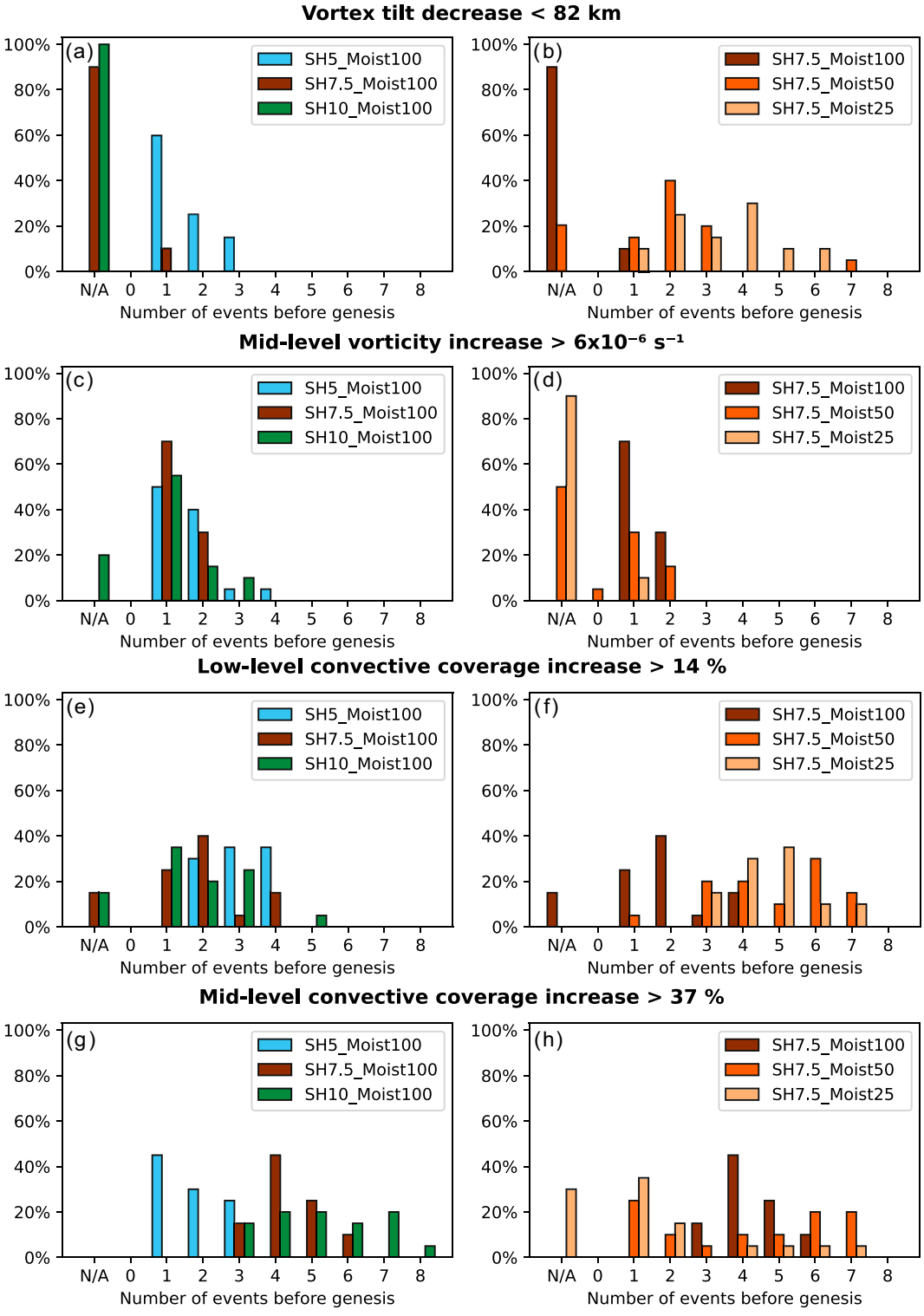

FIG. 11. Histograms of the number of TC genesis precursor events occurring before the timing of genesis. (a),(c),(e),(g) Histograms for Moist100 simulations, composited by shear magnitude. (b),(d),(f),(h) Histograms for SH7.5 simulations, composited by environmental moisture magnitude. Each event is counted with the precursor parameter keeping its value above or below the threshold (Fig. 9) for 3 h continuously. Not applicable (N/A) bin is for the simulations that reached genesis without surpassing the thresholds for the precursor variables.

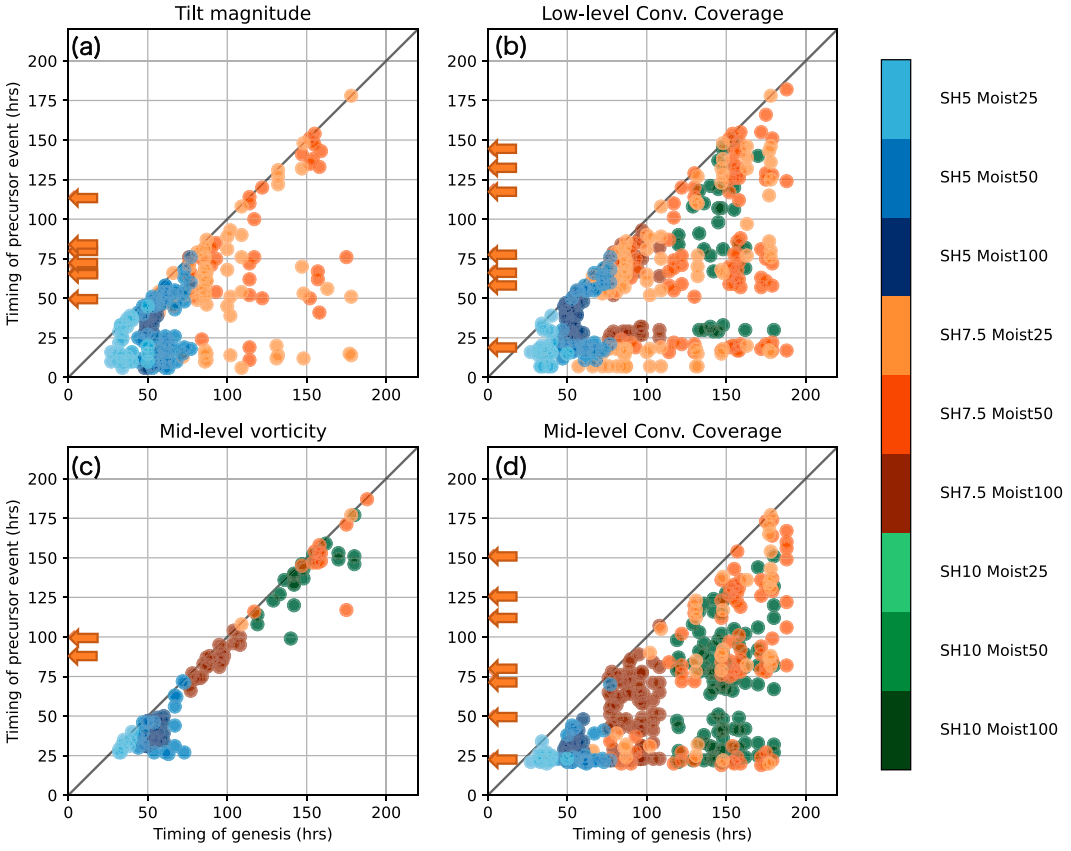

FIG. 12. Timing of the TC genesis precursor events compared to the timing of genesis. Each event is counted with the precursor parameter keeping its value above or below the threshold (Fig. 9) for 3 h continuously. The orange arrows indicate the median time of the first, second, …, and seventh (if any) precursor events for 60 members of the three SH7.5 sets.

set exhibited a unique distribution of precursor event cycles that a TC must undergo before intensifying. The complex and chaotic nature of TC–VWS–dry air interactions, particularly around the convective bursts and the vortex alignment process, was evident in these results. However, we also observed a consistent and steady increase in accumulated vorticity and column saturation fraction. These results demonstrate the multifaceted and intricate mechanisms involved in TC intensification under moderately sheared and dry environments.

d. Time-lagged correlation analysis

The different distribution of the timing of each precursor event before the timing of genesis (Fig. 12) warrants a further investigation of the time order among the physical processes that are represented by the precursor variables. Here we present time-lagged cross-correlation analysis results. Time-lagged cross correlation refers to the correlation between two time series that are shifted in time relative to one another.

Figure 13 shows time-lagged correlations between the time series of 217 h of hourly MSLP and the precursor variables (vortex tilt, midlevel inner-core average vorticity, and low- and midlevel inner-core convective coverage) of the 20 ensembles of SH7.5_Moist50. Vortex tilt should have a positive correlation with MSLP, for tilt decreases as MSLP decreases. Vorticities and convective coverages should have a negative correlation with MSLP because they increase as MSLP drops. Shifting the time series hour by hour, we can find a time lag that records a maximum (vortex tilt) or minimum (vorticity and convective coverage) correlation with MSLP (red dotted lines in Fig. 13). The red solid line denotes the mean time lag from 16 members of SH7.5_Moist50. Four members that have TC genesis after 168 h were excluded to ensure at least 48 h offset from the end of simulation hours given the −72- to +72-h offset kernel (gray lines in Fig. 13).

A positive time lag means the time series of the precursor variable leads the time series of MSLP, which implies predictability for TC intensification. Among the four precursor variables, midlevel convective coverage has the longest mean lead time. However, midlevel convective coverage has a larger variance from member to member compared to the other three variables, which could be interpreted as a less reliable predictor. The reason why the time lag of midlevel convective coverage and MSLP has a large variance is because these time-lagged correlations (Fig. 13d) have two distinctive modes at around 12 and 72 h of lead time, unlike the other variables that have a single peak (vortex tilt) or a single trough (midlevel vorticity and low-level

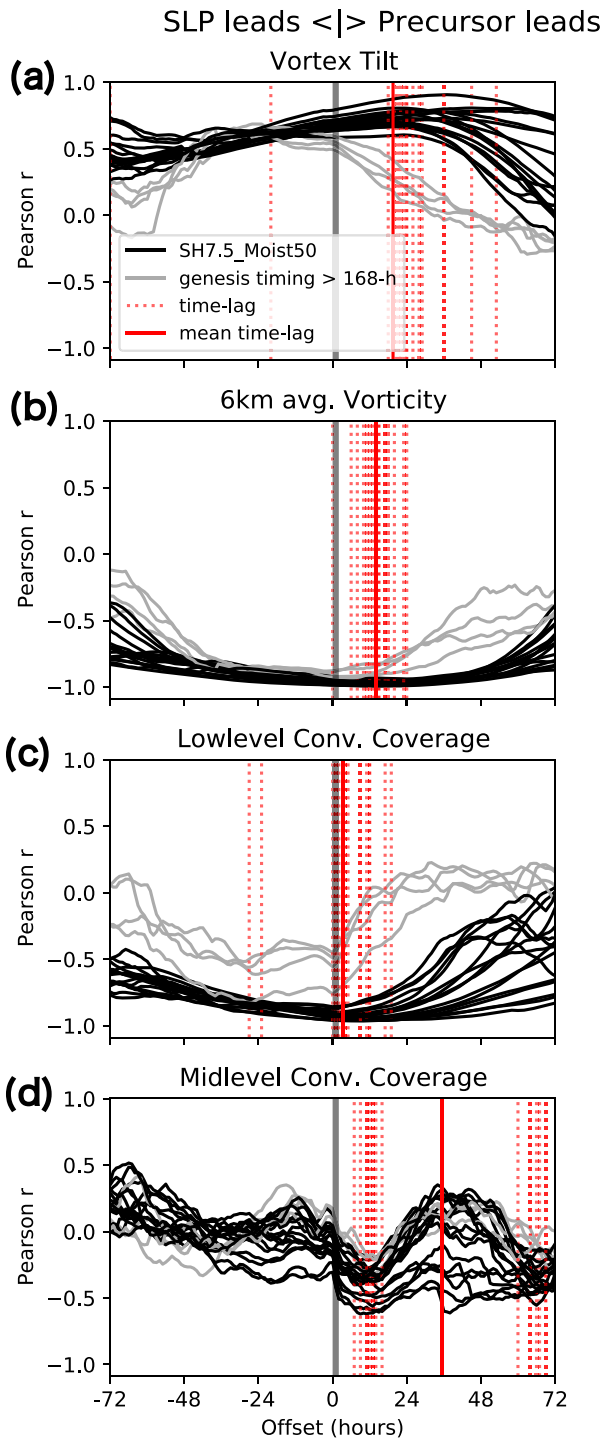

FIG. 13. Time-lagged Pearson correlations between time series of minimum sea level pressure (MSLP) and (a) vortex tilt, (b) midlevel vorticity, (c) low-level convective coverage, and (d) midlevel convective coverage for the SH7.5_Moist50 experimental set. Red dotted vertical lines indicate the time lag of maximum and minimum correlation for each ensemble member. Red solid lines indicate the mean time lag for the members with genesis timing ≤ 168 h. Positive time lag means each precursor event happens before SLP drops below 996-hPa threshold and vice versa.

convective coverage). Among the four variables in Fig. 13, the midlevel vorticity has the best correlation and the narrowest spread of the time lag for SH7.5_Moist50 ensembles, but it has a shorter mean lead time of 12 h.

The wavelike pattern (multiple peaks and troughs) of cross correlations between midlevel convective coverage and SLP is found not only from SH7.5_Moist50 ensemble members but also from other ensembles (Fig. 14). The wavy pattern is thought to be related to multiple incidences of convective bursts. For some members, the two or more local minima of correlations have similar values such that identifying the time lag becomes somewhat uncertain (Figs. 14e,f). Comparing the 3 × 3 panels in Fig. 14, there is a trend that the ensembles from more favorable setups (e.g., SH5_Moist100) have a longer lead time of the midlevel convective coverage, better correlation, and a narrower ensemble spread. On the contrary, the ensemble that had the widest spread in SLP (i.e., SH7.5_Moist50) also exhibits a large ensemble spread in time-lag distributions. The 3 × 3 figures like Fig. 14 for the three other precursor variables can be found in supplemental Figs. 1–3 and they show similar patterns as Figs. 13a–c with a single peak or trough.

Figure 15 summarizes the results of time-lagged cross-correlation analysis for all four precursor variables in one plot. The ensemble-mean time lag is on the y axis, and the standard deviation of the time lags is on the x axis, such that the upper-left corner denotes the best predictor for TC intensification with a long lead time and good confidence. The marker size is proportional to the ensemble mean time-lagged correlation value. Some ensemble members of SH10_Moist100 did not have a statistically significant correlation between midlevel convective coverage and MSLP at 95% confidence level based on a two-sided Student's t test; thus, it is marked with × instead of ◯ (see Figs. 14a and 15d).

In Fig. 15, we observe that the more favorable setups, characterized by smaller VWS and moister environments, generally exhibit metrics with longer lead times, less spread, and better correlations with MSLP evolution, in general. Among the four variables of precursor events, the order of mean lead time is 1) midlevel convective coverage, 2) vortex tilt, 3) low-level convective coverage, and 4) midlevel vorticity. The longer lead time, the smaller correlation, and the larger standard deviation of the midlevel convective coverage with MSLP imply that midlevel convective coverage increasing (that usually happens 48 h before TC genesis) does not always end up with TC intensification. Higher correlation and smaller ensemble spread of midlevel vorticity mean that midlevel vorticity increasing (that usually happens 12 h before TC genesis) has a better chance of resulting in imminent TC intensification compared to midlevel convective coverage increasing. However, it is important to note that despite these statistical trends, our analyses have revealed overlaps between circles and similar lead times for different variables, as depicted in both Figs. 12 and 15. This analysis indicates that the time order of these precursor events is not easily separable and highlights the uncertainties in causal relationships leading to TC intensification. The time order of each precursor event and the probability of each precursor event eventually leading to TC intensification are further discussed in section 4.

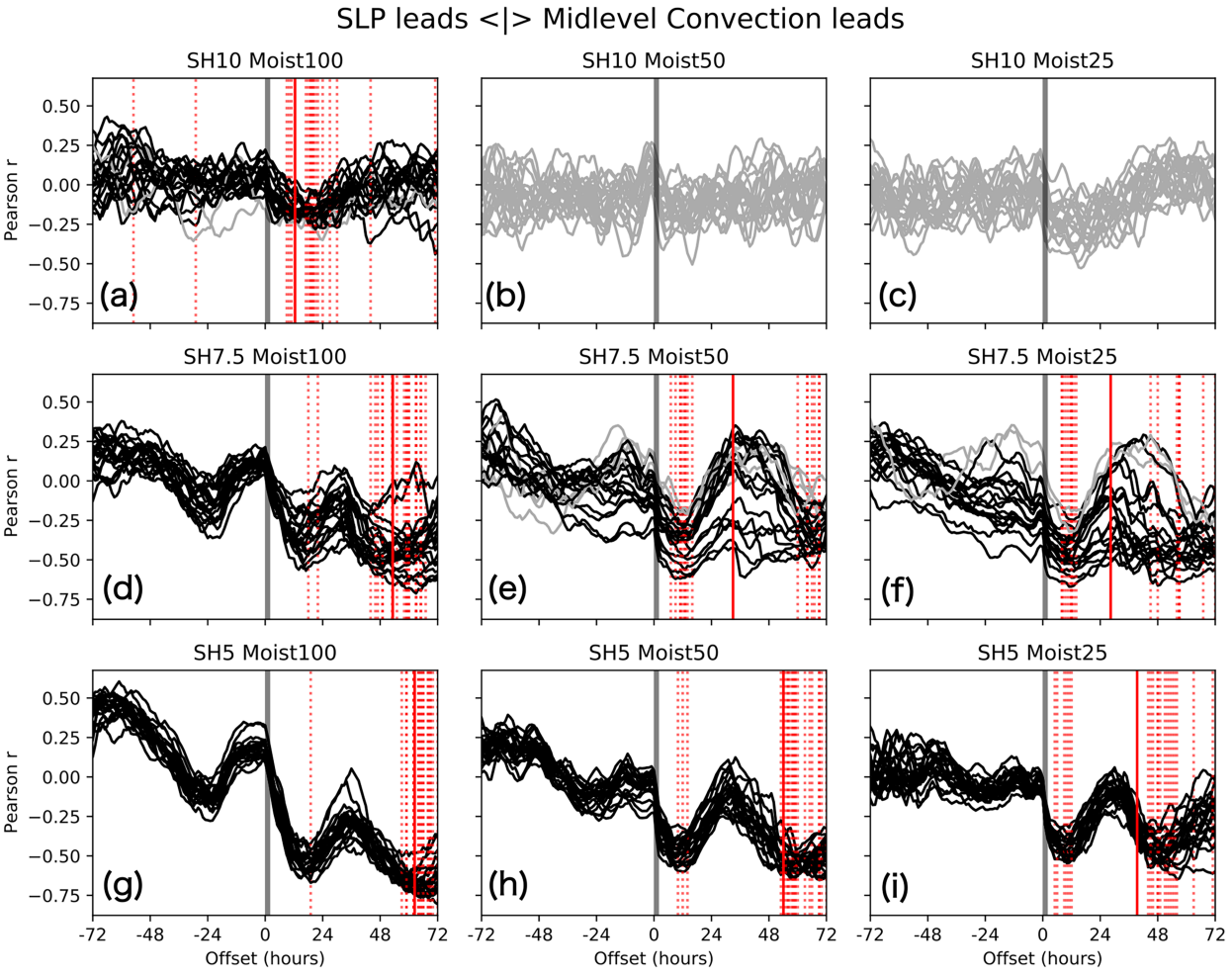

FIG. 14. Time-lag Pearson correlation between time series of MSLP and midlevel convective coverage as a function of time lag for the whole nine sets of experiments. Annotation is as in Fig. 13.

4. Discussion and conclusions

Our extensive mesoscale ensemble modeling demonstrates that marginally favorable environments, characterized by moderate magnitudes of VWS and intermediate levels of humidity (SH7.5_Moist50 and SH7.5_Moist25), are associated with the highest level of uncertainty in tropical cyclone genesis and intensification, consistent with previous literature (Alland et al. 2021a; Tao and Zhang 2014). A key finding was that there are repetitive cycles of precursor events lining up together before TC intensification, and slow- or nondeveloping ensemble members of the marginal environments go through a number of the cycles of precursor events that are very close to successful ones.

Based on the close examination of selected ensemble members and statistical analysis of probabilities of precursor events and time-lagged correlations, we propose a diagram that represents the hierarchy of the processes leading into tropical cyclone intensification in sheared and dry environments (Fig. 16).

The first floor of the pyramid in Fig. 16 is synoptic-scale favorable thermodynamic conditions. Gray (1979) showed that a moist atmosphere and a well-mixed, warm oceanic layer serve as necessary conditions for TC genesis. We prescribed warm SSTs of 29°C, and all 180 simulations spent the first 24–36 h of incubation time to moisten the inner-core region (Fig. 10). The second floor is the existence of closed mesoscale low-level circulation. We initialized the simulations with a weak vortex centered at 850 hPa. Low-level closed circulation is one of the first signals of intensification found from tropical disturbances in the range of "Invest" and TD (Nam and Bell 2021; Wang et al. 2012). After the first two floors set the stage for synoptic- to meso-alpha-scale environments, on the third floor, there emerges a wider area of deep convection (captured by increasing signals of midlevel and low-level convective coverage parameters). Inside the deep organized mesoscale convective system, a new midlevel vortex forms inside the broader preexisting midlevel circulation (Fig. 7), which results in rapid vortex tilt decrease: the fourth floor of the pyramid. The fifth floor is sustained vertical alignment of the newly reformed midlevel vortex and the low-level vortex. If the newly reformed midlevel vortex becomes firmly aligned with the low-level vortex, the vortex tower can be resilient against VWS (Schecter and Montgomery 2003;

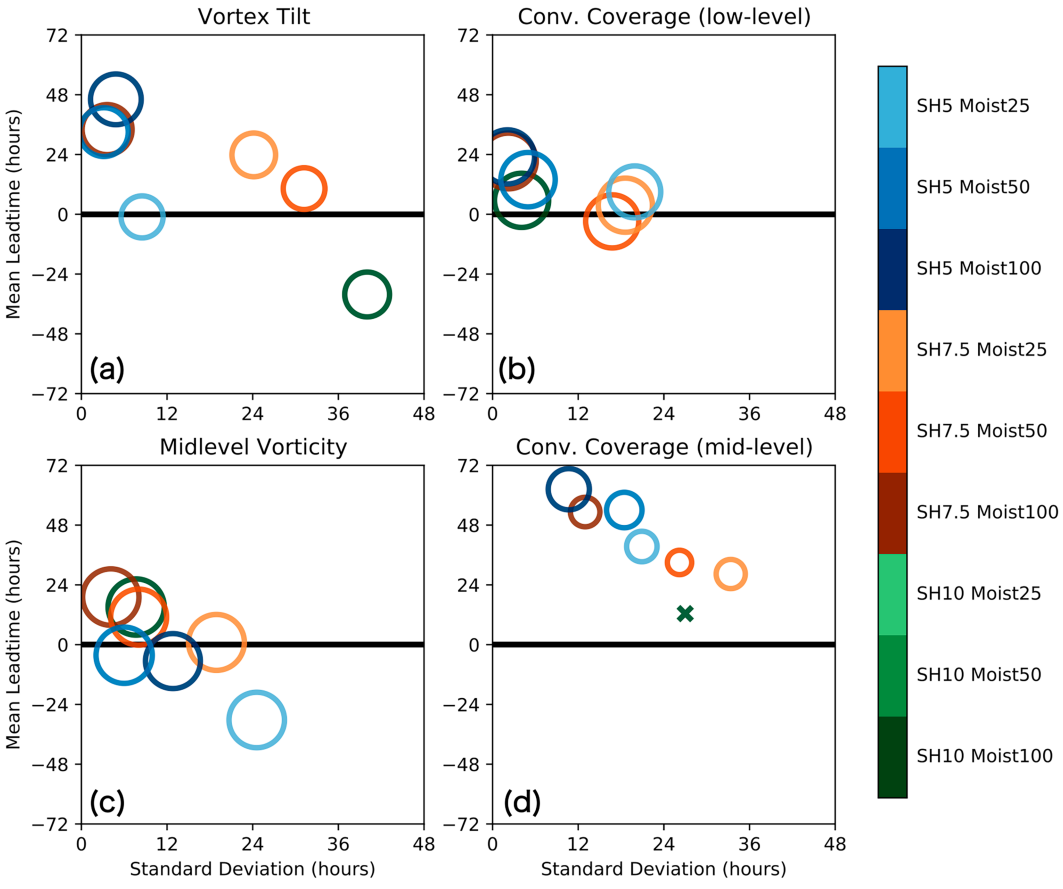

FIG. 15. Time-lag correlation analysis results for the time series of MSLP and each of the four precursor variables with a mean of time lag for the y axis and standard deviation of the time lag of 20 ensemble members on the x axis. The size of the circle is proportional to the mean correlation between two time series at the time lag. The combination that had a correlation not significant at 95% level is marked with × rather than a circle. The ensemble sets that do not have any developing members are not shown.

Reasor et al. 2004). In our analysis, the vortex alignment process manifests as the tilt keeps decreasing with some fluctuation (e.g., 100–125 h of the early-developing member and 150–175 h of the late-developing member from SH7.5_Moist50 in Fig. 3). If the fifth floor was successful, vortex tilt keeps decreasing, and the deep convection that is centered around the midlevel center organizes itself near the low-level center: the sixth floor. Then, the midlevel vortex intensifies, as captured by midlevel vorticity increasing, and the simulated vortex finally reaches the pinnacle of the pyramid and the TC intensifies.

In this study, we expand our knowledge of the dynamic and thermodynamic processes that lead to TC intensification in sheared and dry environments by showing the probabilistic distribution of the precursor events and identifying the critical processes that serve as the bifurcation points between the developing and nondeveloping vortices in the course of the repetitive cycles of precursor events. The ensemble sets that have a narrower ensemble spread (small VWS and high humidity) need only a few cycles of precursor events, but the ensemble sets that have a wider ensemble spread have some members developing after one or two cycles and other members developing after seven to eight cycles of precursor events repeating with a 24–48-h period (Fig. 11). We suggest that the widespread distribution of the number of precursor events is related to the lower success rate of each precursor event. Whether each cycle of precursor events is successful for TC genesis or not is somewhat random due to the stochastic characteristic of convective-scale phenomena, but the probability of success of each cycle can increase with time as the environment becomes moister and more favorable with each cycle (Fig. 5 versus Fig. 8).

The critical bifurcation point in these experiments appears to be the fifth floor of the pyramid, the sustained vortex alignment process, for SH7.5_Moist50 and SH7.5_Moist25 set. Before TC genesis, midlevel convective coverage increases, and vortex tilt decreases multiple times (Fig. 12). These variables have a longer lead time with a smaller correlation and larger standard deviation (Fig. 15). This means that not all events of midlevel convective coverage increasing and vortex tilt decreasing result in low-level convective coverage increasing or midlevel vorticity increasing. From these results, we infer that most of the late-developing members of SH7.5_Moist50 fail at

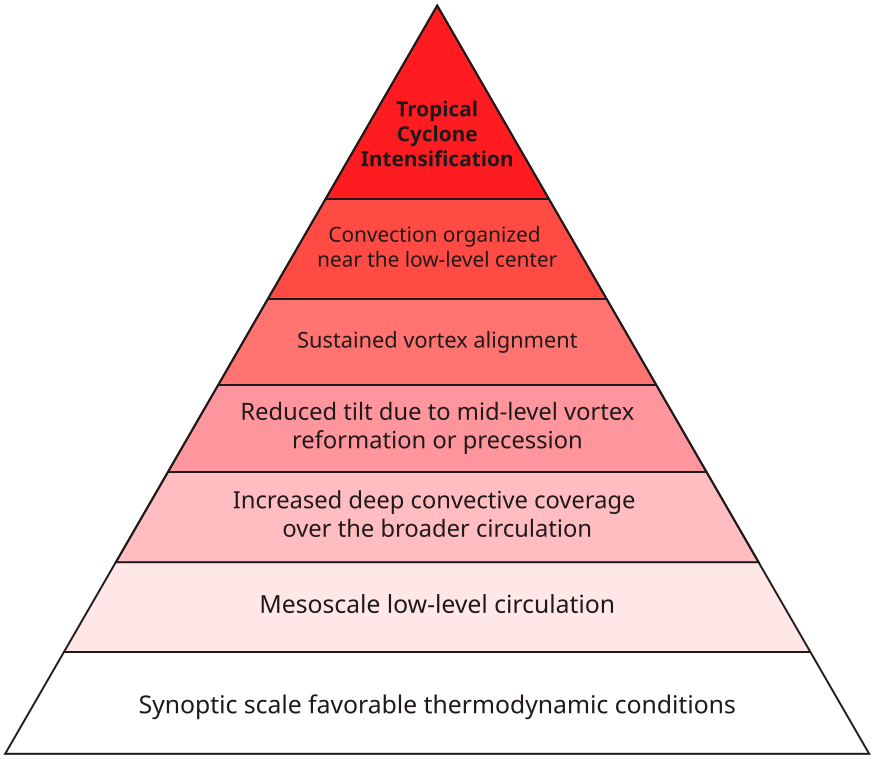

FIG. 16. A pyramid diagram of tropical cyclone (TC) intensification in moderately sheared and dry environments. The diagram shows the hierarchy of the precursor events leading to TC intensification for a lower floor condition should be satisfied for the TC to move on to the next upper floor of the pyramid. There could be multiple trials to satisfy the condition on each floor and TCs can climb up the pyramid to go closer to intensification onset or descend and move farther away from the pinnacle.

the sustained vortex alignment process; there is a newly reformed meso-beta-scale midlevel vortex close to the existing meso-alpha-scale low-level center, but the midlevel vortex is advected downshear swiftly before the vortices in different vertical layers align and grow resilient against VWS. Then, the vortex tilt increases again, and the cycle resets, going back to the third floor of the pyramid again. While our statistical and probabilistic analyses provide insights into the time order of events, the overlaps in the lead time and large variances also demonstrate the intricate challenges of disentangling the precise timing and causal relationships between the various precursor events.

We could not pinpoint the difference between the midlevel vortex that can maintain sustained vortex alignment with the low-level vortex versus the ones that are carried away. We looked at the location of deep convection in shear quadrants, the location of the newly formed midlevel vortex with regard to the low-level vortex center, and stratiform coverage (see supplemental Fig. 6), but some cases exhibited very similar patterns, yet one underwent TC genesis and the other failed. Nevertheless, we can infer from saturation fraction analysis and midlevel vortex cross sections that a midlevel vortex that is formed closer to the low-level center with a larger spatial scale and a moister environment helps sustain the vortex alignment process. We observed cyclonic movement of deep convection from the downshear to downshear-left direction prior to the rapid decrease in tilt for both the earliest- and latest-developing members (supplemental Fig. 6). This observation is consistent with previous studies (e.g., Rios-Berrios et al. 2018), suggesting that the asymmetric distribution of moisture and convection relative to shear direction could be another significant distinction between developers and nondevelopers. Additional research is required to better understand the factors that lead to sustained vortex alignment in the presence of VWS and dry air.

This research aimed to identify the sources of increased uncertainty of tropical cyclone intensification in marginally favorable environments through the understanding of the key multiscale precursors leading to tropical cyclogenesis and intensification in such environments. Based on the results herein, the uncertainty can be largely attributed to the probabilistic characteristics of precursor events lining up together before TC genesis and intensification. In an extremely favorable or hostile environment, the success rate of each precursor event is either very high or very low, so the probability of ultimate TC intensification is skewed to 1 or 0. However, in a marginal environment, the success rate is moderate such that a TC can undergo TC genesis and continuous intensification

with a first trial, or it could exhibit robust signals such as deep convective organization or low-level closed circulation but still fail to intensify. In reality, the environmental conditions change; thus, a system that requires multiple repetitions of precursor events could miss the window of opportunity and dissipate as the environment becomes more hostile. On the other hand, some systems could develop into a TC climbing up the pyramid rapidly after entering a more favorable environment like the case of Hagupit (2008) (Nam and Bell 2021).

Our idealized simulations simplify the variable space by having the other variables constant to isolate the impacts of varying VWS and environmental humidity. In reality, there is a lot more complexity that contributes to the uncertainty around TC genesis and intensification, such as land–TC interaction (Alvey et al. 2022). We conducted additional experiments to investigate sensitivity to different types of the initial vortex (midlevel centered and weaker vortex) and choices of radiation and microphysics schemes (long- and shortwave radiation and Thompson microphysics). The preliminary analysis of these sensitivity test experiments showed that all successfully developing TCs shared these common precursor events as described in Fig. 16 while the critical bifurcation points of success and failed intensification cases were different depending on the experiments. For example, midlevel centered vortices in 7.5 m s^{-1} of VWS and Moist50 setups had an even larger ensemble spread than the low-level centered vortices in SH7.5_Moist50 shown here, and the late-developing members of the midlevel sensitivity test failed at the midlevel vortex reformation process (fourth floor of the diagram), not the sustained alignment process (fifth floor of the diagram). Our findings from the sensitivity tests will be reported in a subsequent study, which will continue to bridge the gap between the idealized simulations shown herein and the more complex reality of the tropical atmosphere.

Acknowledgments. The authors thank Eric Maloney, Steve Rutledge, Brian Tang, and two anonymous reviewers for their helpful comments. This research was funded by Office of Naval Research Awards N000141613033 and N000142012069. Computational resources were provided by XSEDE Allocation TG-ATM190001.

Data availability statement. The high-resolution model outputs that support the findings of this study are too large and stored in local computer clusters, thus are only available on request from the corresponding author, CCN, but the key input files to reproduce the simulations are available at https://doi.org/10.5281/zenodo.6476490.

REFERENCES

Alland, J. J., B. H. Tang, and K. L. Corbosiero, 2017: Effects of midlevel dry air on development of the axisymmetric tropical cyclone secondary circulation. *J. Atmos. Sci.*, **74**, 1455–1470, https://doi.org/10.1175/JAS-D-16-0271.1.

——, ——, ——, and G. H. Bryan, 2021a: Combined effects of midlevel dry air and vertical wind shear on tropical cyclone development. Part I: Downdraft ventilation. *J. Atmos. Sci.*, **78**, 763–782, https://doi.org/10.1175/JAS-D-20-0054.1.

——, ——, ——, and ——, 2021b: Combined effects of midlevel dry air and vertical wind shear on tropical cyclone development. Part II: Radial ventilation. *J. Atmos. Sci.*, **78**, 783–796, https://doi.org/10.1175/JAS-D-20-0055.1.

Alvey, G. R., III, and A. Hazelton, 2022: How do weak, misaligned tropical cyclones evolve toward alignment? A multicase study using the Hurricane Analysis and Forecast System. *J. Geophys. Res. Atmos.*, **127**, e2022JD037268, https://doi.org/10.1029/2022JD037268.

——, M. Fischer, P. Reasor, J. Zawislak, and R. Rogers, 2022: Observed processes underlying the favorable vortex repositioning early in the development of Hurricane Dorian (2019). *Mon. Wea. Rev.*, **150**, 193–213, https://doi.org/10.1175/MWR-D-21-0069.1.

Bell, M. M., and M. T. Montgomery, 2019: Mesoscale processes during the genesis of Hurricane Karl (2010). *J. Atmos. Sci.*, **76**, 2235–2255, https://doi.org/10.1175/JAS-D-18-0161.1.

Bhatia, K. T., and D. S. Nolan, 2013: Relating the skill of tropical cyclone intensity forecasts to the synoptic environment. *Wea. Forecasting*, **28**, 961–980, https://doi.org/10.1175/WAF-D-12-00110.1.

Bracken, W. E., and L. F. Bosart, 2000: The role of synoptic-scale flow during tropical cyclogenesis over the North Atlantic Ocean. *Mon. Wea. Rev.*, **128**, 353–376, https://doi.org/10.1175/1520-0493(2000)128<0353:TROSSF>2.0.CO;2.

Chavas, D. R., K. A. Reed, and J. A. Knaff, 2017: Physical understanding of the tropical cyclone wind-pressure relationship. *Nat. Commun.*, **8**, 1360, https://doi.org/10.1038/s41467-017-01546-9.

Chen, X., Y. Wang, J. Fang, and M. Xue, 2018: A numerical study on rapid intensification of Typhoon Vicente (2012) in the South China Sea. Part II: Roles of inner-core processes. *J. Atmos. Sci.*, **75**, 235–255, https://doi.org/10.1175/JAS-D-17-0129.1.

Courtney, J., and J. A. Knaff, 2009: Adapting the Knaff and Zehr wind-pressure relationship for operational use in tropical cyclone warning centres. *Aust. Meteor. Oceanogr. J.*, **58**, 167–179, https://doi.org/10.22499/2.5803.002.

Davis, C. A., and D. A. Ahijevych, 2013: Thermodynamic environments of deep convection in Atlantic tropical disturbances. *J. Atmos. Sci.*, **70**, 1912–1928, https://doi.org/10.1175/JAS-D-12-0278.1.

Dunion, J. P., 2011: Rewriting the climatology of the tropical North Atlantic and Caribbean Sea atmosphere. *J. Climate*, **24**, 893–908, https://doi.org/10.1175/2010JCLI3496.1.

——, and C. S. Marron, 2008: A reexamination of the Jordan mean tropical sounding based on awareness of the Saharan air layer: Results from 2002. *J. Climate*, **21**, 5242–5253, https://doi.org/10.1175/2008JCLI1868.1.

——, C. D. Thorncroft, and C. S. Velden, 2014: The tropical cyclone diurnal cycle of mature hurricanes. *Mon. Wea. Rev.*, **142**, 3900–3919, https://doi.org/10.1175/MWR-D-13-00191.1.

Finocchio, P. M., and S. J. Majumdar, 2017: The predictability of idealized tropical cyclones in environments with time-varying vertical wind shear. *J. Adv. Model. Earth Syst.*, **9**, 2836–2862, https://doi.org/10.1002/2017MS001168.

Gray, W. M., 1979: Hurricanes: Their formation, structure and likely role in the tropical circulation. *Meteorology over the Tropical Oceans*, D. B. Shaw, Ed., James Glaisher House, 155–218.

Hong, S.-Y., J. Dudhia, and S.-H. Chen, 2004: A revised approach to ice microphysical processes for the bulk parameterization of clouds and precipitation. *Mon. Wea. Rev.*, **132**, 103–120, https://doi.org/10.1175/1520-0493(2004)132<0103:ARATIM>2.0.CO;2.

——, Y. Noh, and J. Dudhia, 2006: A new vertical diffusion package with an explicit treatment of entrainment processes. *Mon. Wea. Rev.*, **134**, 2318–2341, https://doi.org/10.1175/MWR3199.1.

James, R. P., and P. M. Markowski, 2010: A numerical investigation of the effects of dry air aloft on deep convection. *Mon. Wea. Rev.*, **138**, 140–161, https://doi.org/10.1175/2009MWR3018.1.

Judt, F., S. S. Chen, and J. Berner, 2016: Predictability of tropical cyclone intensity: Scale-dependent forecast error growth in high-resolution stochastic kinetic-energy backscatter ensembles. *Quart. J. Roy. Meteor. Soc.*, **142**, 43–57, https://doi.org/10.1002/qj.2626.

Klotzbach, P. J., M. M. Bell, S. G. Bowen, E. J. Gibney, K. R. Knapp, and C. J. Schreck III, 2020: Surface pressure a more skillful predictor of normalized hurricane damage than maximum sustained wind. *Bull. Amer. Meteor. Soc.*, **101**, E830–E846, https://doi.org/10.1175/BAMS-D-19-0062.1.

Knaff, J. A., and R. M. Zehr, 2007: Reexamination of tropical cyclone wind–pressure relationships. *Wea. Forecasting*, **22**, 71–88, https://doi.org/10.1175/WAF965.1.

Lorenz, E. N., 1969: The predictability of a flow which possesses many scales of motion. *Tellus*, **21**, 289–307, https://doi.org/10.3402/tellusa.v21i3.10086.

Martinez, J., C. C. Nam, and M. M. Bell, 2020: On the contributions of incipient vortex circulation and environmental moisture to tropical cyclone expansion. *J. Geophys. Res. Atmos.*, **125**, e2020JD033324, https://doi.org/10.1029/2020JD033324.

Melhauser, C., and F. Zhang, 2012: Practical and intrinsic predictability of severe and convective weather at the mesoscales. *J. Atmos. Sci.*, **69**, 3350–3371, https://doi.org/10.1175/JAS-D-11-0315.1.

Montgomery, M. T., and Coauthors, 2012: The Pre-Depression Investigation of Cloud-Systems in the Tropics (PREDICT) experiment: Scientific basis, new analysis tools, and some first results. *Bull. Amer. Meteor. Soc.*, **93**, 153–172, https://doi.org/10.1175/BAMS-D-11-00046.1.

Moon, Y., and D. S. Nolan, 2010: Do gravity waves transport angular momentum away from tropical cyclones? *J. Atmos. Sci.*, **67**, 117–135, https://doi.org/10.1175/2009JAS3088.1.

Murthy, V. S., and W. R. Boos, 2018: Role of surface enthalpy fluxes in idealized simulations of tropical depression spinup. *J. Atmos. Sci.*, **75**, 1811–1831, https://doi.org/10.1175/JAS-D-17-0119.1.

Nam, C. C., 2021: Multi-scale interactions leading to tropical cyclogenesis in sheared environments. Ph.D. thesis, Colorado State University, 134 pp.

——, and M. M. Bell, 2021: Multiscale shear impacts during the genesis of Hagupit (2008). *Mon. Wea. Rev.*, **149**, 551–569, https://doi.org/10.1175/MWR-D-20-0133.1.

Nguyen, L. T., and J. Molinari, 2015: Simulation of the downshear reformation of a tropical cyclone. *J. Atmos. Sci.*, **72**, 4529–4551, https://doi.org/10.1175/JAS-D-15-0036.1.

——, ——, and D. Thomas, 2014: Evaluation of tropical cyclone center identification methods in numerical models. *Mon. Wea. Rev.*, **142**, 4326–4339, https://doi.org/10.1175/MWR-D-14-00044.1.

Nolan, D. S., 2011: Evaluating environmental favorableness for tropical cyclone development with the method of point-downscaling. *J. Adv. Model. Earth Syst.*, **3**, M08001, https://doi.org/10.1029/2011MS000063.

——, and M. G. McGauley, 2012: Tropical cyclogenesis in wind shear: Climatological relationships and physical processes. *Cyclones: Formation, Triggers, and Control*, K. Oouchi and H. Fudeyasu, Eds., Nova Science Publishers, 1–35.

——, E. D. Rappin, and K. A. Emanuel, 2007: Tropical cyclogenesis sensitivity to environmental parameters in radiative–convective equilibrium. *Quart. J. Roy. Meteor. Soc.*, **133**, 2085–2107, https://doi.org/10.1002/qj.170.

Ooyama, K. V., 1982: Conceptual evolution of the theory and modeling of the tropical cyclone. *J. Meteor. Soc. Japan*, **60**, 369–380, https://doi.org/10.2151/jmsj1965.60.1_369.

Peng, M. S., B. Fu, T. Li, and D. E. Stevens, 2012: Developing versus nondeveloping disturbances for tropical cyclone formation. Part I: North Atlantic. *Mon. Wea. Rev.*, **140**, 1047–1066, https://doi.org/10.1175/2011MWR3617.1.

Raymond, D. J., and G. Kilroy, 2019: Control of convection in high-resolution simulations of tropical cyclogenesis. *J. Adv. Model. Earth Syst.*, **11**, 1582–1599, https://doi.org/10.1029/2018MS001576.

——, S. Gjorgjievska, S. Sessions, and Ž. Fuchs, 2014: Tropical cyclogenesis and mid-level vorticity. *Aust. Meteor. Oceanogr. J.*, **64**, 11–25, https://doi.org/10.22499/2.6401.003.

Reasor, P. D., M. T. Montgomery, and L. D. Grasso, 2004: A new look at the problem of tropical cyclones in vertical shear flow: Vortex resiliency. *J. Atmos. Sci.*, **61**, 3–22, https://doi.org/10.1175/1520-0469(2004)061<0003:ANLATP>2.0.CO;2.

Riemer, M., M. T. Montgomery, and M. E. Nicholls, 2010: A new paradigm for intensity modification of tropical cyclones: Thermodynamic impact of vertical wind shear on the inflow layer. *Atmos. Chem. Phys.*, **10**, 3163–3188, https://doi.org/10.5194/acp-10-3163-2010.

Rios-Berrios, R., 2020: Impacts of radiation and cold pools on the intensity and vortex tilt of weak tropical cyclones interacting with vertical wind shear. *J. Atmos. Sci.*, **77**, 669–689, https://doi.org/10.1175/JAS-D-19-0159.1.

——, and R. D. Torn, 2017: Climatological analysis of tropical cyclone intensity changes under moderate vertical wind shear. *Mon. Wea. Rev.*, **145**, 1717–1738, https://doi.org/10.1175/MWR-D-16-0350.1.

——, ——, and C. A. Davis, 2016: An ensemble approach to investigate tropical cyclone intensification in sheared environments. Part II: Ophelia (2011). *J. Atmos. Sci.*, **73**, 1555–1575, https://doi.org/10.1175/JAS-D-15-0245.1.

——, C. A. Davis, and R. D. Torn, 2018: A hypothesis for the intensification of tropical cyclones under moderate vertical wind shear. *J. Atmos. Sci.*, **75**, 4149–4173, https://doi.org/10.1175/JAS-D-18-0070.1.

Rogers, R. F., P. D. Reasor, and J. A. Zhang, 2015: Multiscale structure and evolution of Hurricane Earl (2010) during rapid intensification. *Mon. Wea. Rev.*, **143**, 536–562, https://doi.org/10.1175/MWR-D-14-00175.1.

Schecter, D. A., and M. T. Montgomery, 2003: On the symmetrization rate of an intense geophysical vortex. *Dyn. Atmos. Oceans*, **37**, 55–88, https://doi.org/10.1016/S0377-0265(03)00015-0.

——, and K. Menelaou, 2020: Development of a misaligned tropical cyclone. *J. Atmos. Sci.*, **77**, 79–111, https://doi.org/10.1175/JAS-D-19-0074.1.

Skamarock, W. C., and Coauthors, 2008: A description of the Advanced Research WRF version 3. NCAR Tech. Note NCAR/TN-475+STR, 113 pp., https://doi.org/10.5065/D68S4MVH.

Tang, B., and K. Emanuel, 2012: Sensitivity of tropical cyclone intensity to ventilation in an axisymmetric model. *J. Atmos. Sci.*, **69**, 2394–2413, https://doi.org/10.1175/JAS-D-11-0232.1.

——, and Coauthors, 2020: Recent advances in research on tropical cyclogenesis. *Trop. Cyclone Res. Rev.*, **9**, 87–105, https://doi.org/10.1016/j.tcrr.2020.04.004.

Tao, D., 2015: Dynamics and predictability of tropical cyclones under vertical wind shear. Ph.D. thesis, The Pennsylvania State University, 173 pp.

——, and F. Zhang, 2014: Effect of environmental shear, sea-surface temperature, and ambient moisture on the formation

and predictability of tropical cyclones: An ensemble-mean perspective. *J. Adv. Model. Earth Syst.*, **6**, 384–404, https://doi.org/10.1002/2014MS000314.

——, and ——, 2015: Effects of vertical wind shear on the predictability of tropical cyclones: Practical versus intrinsic limit. *J. Adv. Model. Earth Syst.*, **7**, 1534–1553, https://doi.org/10.1002/2015MS000474.

Wang, Z., 2012: Thermodynamic aspects of tropical cyclone formation. *J. Atmos. Sci.*, **69**, 2433–2451, https://doi.org/10.1175/JAS-D-11-0298.1.

——, M. T. Montgomery, and C. Fritz, 2012: A first look at the structure of the wave pouch during the 2009 PREDICT–GRIP dry runs over the Atlantic. *Mon. Wea. Rev.*, **140**, 1144–1163, https://doi.org/10.1175/MWR-D-10-05063.1.

WMO, 2017: Global guide to tropical cyclone forecasting. WMO Rep. WMO-1194, 399 pp., https://cyclone.wmo.int/pdf/Global-Guide-to-Tropical-Cyclone-Forecasting.pdf.

Zhang, F., and D. Tao, 2013: Effects of vertical wind shear on the predictability of tropical cyclones. *J. Atmos. Sci.*, **70**, 975–983, https://doi.org/10.1175/JAS-D-12-0133.1.